Contrib Mineral Petrol (1999) 137: 304–322

R. Altherr · F. Henjes-Kunst · C. Langer · J. Otto

Interaction between crustal-derived felsic and mantle-derived mafic magmas in the Oberkirch Pluton (European Variscides, Schwarzwald, Germany)

Received: 30 April 1999 / Accepted: 6 August 1999

Abstract The composite Oberkirch pluton consists of three compositionally different units of peraluminous biotite granite. The northern unit is relatively mafic (SiO_2 ~64%) and lacks cordierite. The more felsic central and southern units (SiO_2 = 67.8 to 70.4%) can only be distinguished from each other by the occurrence of cordierite in the former. Mafic microgranular enclaves of variable composition, texture and size occur in each of these units and are concentrated in their central domains. Most abundant are large (dm to m) hornblende-bearing enclaves with dioritic to tonalitic compositions (SiO_2 = 50.8 to 56.3 wt%; Mg# = 63 to 41) and fine grained doleritic textures that suggest chilling against the host granite magma. Some of these enclaves are mantled by hybrid zones. Less common are microtonalitic enclaves containing biotite as the only primary mafic phase (SiO_2 = 53.7 to 64.4%) and small hybrid tonalitic to granodioritic enclaves and schlieren. Synplutonic dioritic dikes (up to 6 m thick) with hybrid transition zones to the host granite occur in the southern unit of the pluton. In chemical variation diagrams, samples from unmodified hornblende-bearing mafic enclaves and dikes form continuous trends that are compatible with an origin by fractionation of olivine, clinopyroxene, hornblende and plagioclase. Chemical and initial isotopic signatures (e.g. high Mg#, low Na_2O, $\varepsilon_{Nd} = -1.2$ to -5.1, $^{87}Sr/^{86}Sr = 0.7055$ to 0.7080, $\delta^{18}O = 8.0$ to 8.8‰) exclude an origin by partial melting from a mafic meta-igneous source but favour derivation from a heterogeneous enriched lithospheric mantle. Samples from the granitic host rocks do not follow the chemical variation trends defined by the diorites but display large scatter. In addition, their initial isotopic characteristics ($\varepsilon_{Nd} = -4.5$ to -6.8, $^{87}Sr/^{86}Sr = 0.7071$ to 0.7115, $\delta^{18}O = 9.9$ to 11.9‰) show little overlap with those of the diorites. Most probably, the granitic magmas were derived from metapelitic sources characterized by variable amounts of garnet and plagioclase. This is suggested by relatively high molar ratios of $Al_2O_3/(MgO + FeO_{tot})$ and K_2O/Na_2O, in combination with low ratios of $CaO/(MgO + FeO_{tot})$, variable values of Sr/Nd, $Eu/Eu^* [= Eu_{cn}/(Sm_{cn} \times Gd_{cn})^{0.5}]$ and $(Tb/Yb)_{cn}$ (cn = chondrite-normalized) as well as variable abundances of Sc and Y. Whole-rock initial isotopic signatures of mafic microtonalitic enclaves ($\varepsilon_{Nd} = -4.6$ to -5.2; $^{87}Sr/^{86}Sr = 0.7060$ to 0.7073; $\delta^{18}O$ ~8.1‰) are similar to those of the low ε_{Nd} diorites. Plagioclase concentrates from a granite sample and a mafic microtonalitic enclave are characterized by initial $^{87}Sr/^{86}Sr$ ratios that are significantly higher than those of their bulk rock systems suggesting incorporation of high $^{87}Sr/^{86}Sr$ crustal material into the magmas. Field relationships and petrographic evidence suggest that the Oberkirch pluton originated by at least three pulses of granitic magma containing mafic magma globules. In-situ hybridization between the different magmas was limited. Late injection of dioritic magma into the almost solidified granitic southern unit resulted in the formation of more or less continuous synplutonic dikes surrounded by relatively thin hybrid zones.

R. Altherr (✉) · C. Langer[1]
Mineralogisches Institut, Universität Heidelberg,
Im Neuenheimer Feld 236, D-69120 Heidelberg, Germany
e-mail: raltherr@classic.min.uni-heidelberg.de
Tel.: +49-6221-548206; Fax: +49-6221-544805

F. Henjes-Kunst
Bundesanstalt für Geowissenschaften und Rohstoffe,
Stilleweg 2, D-30655 Hannover, Germany

J. Otto
Institut für Mineralogie, Petrologie und Geochemie,
Universität Freiburg, Albertstrasse 23b,
D-79104 Freiburg i. Br., Germany

Present address:
[1] Institut für Festkörper-und Werkstofforschung,
Helmholtzstrasse 20, D-01069 Dresden, Germany

Editorial responsibility: J. Hoefs

Introduction

Most granitic plutons are characterized by compositional heterogeneities of different scales, ranging from

crystal zoning via xenocrysts, mafic clots, schlieren, xenoliths, mafic microgranular enclaves, enclave swarms and dikes to pluton zonation. These heterogeneities may arise due to fractional crystallization, entrainment of restite material, contamination, assimilation, multiple intrusions of compositionally different magmas, magma mingling and mixing as well as late-stage diffusion and recrystallization. In many cases, the generation of composite plutons is attributed to interaction between mafic and felsic magmas. The efficiency and spatial extent of thermal, mechanical and chemical exchange between coexisting magmas depend on their physical and chemical properties, mass fractions and the dynamics of the magma system (e.g. Zorpi et al. 1989; Poli and Tommasini 1991; Barbarin and Didier 1992; Van der Laan and Wyllie 1993; Petford et al. 1996).

In this paper, we examine various types of interaction between crustal-derived granitic and mantle-derived dioritic magmas in the Variscan Oberkirch pluton, in Schwarzwald, Germany. Based on petrographic, chemical and Nd-Sr-O isotopic characteristics of representative samples from the various rock types of this composite pluton, we discuss different types of hybridization obtained by multiple injection of mafic magma into the granite system at different stages of crystallization.

Geological setting and main petrographic features

The Oberkirch pluton is located in the Moldanubian zone of the European Variscides (Kossmat 1927). Field relations and petrographic features of the pluton have been described by Otto (1971/72, 1974). The western part of the original pluton is cut off by normal faults of the Tertiary Rhine graben (Fig. 1). In the north and southeast, high-grade metamorphic rocks of the central Schwarzwald Gneiss Complex (CSGC; Eisbacher et al. 1989; Kalt et al. 1994a, 1999; Hanel et al. 1999a, b) form the immediate country rocks. The shape of the contact is irregular and in part

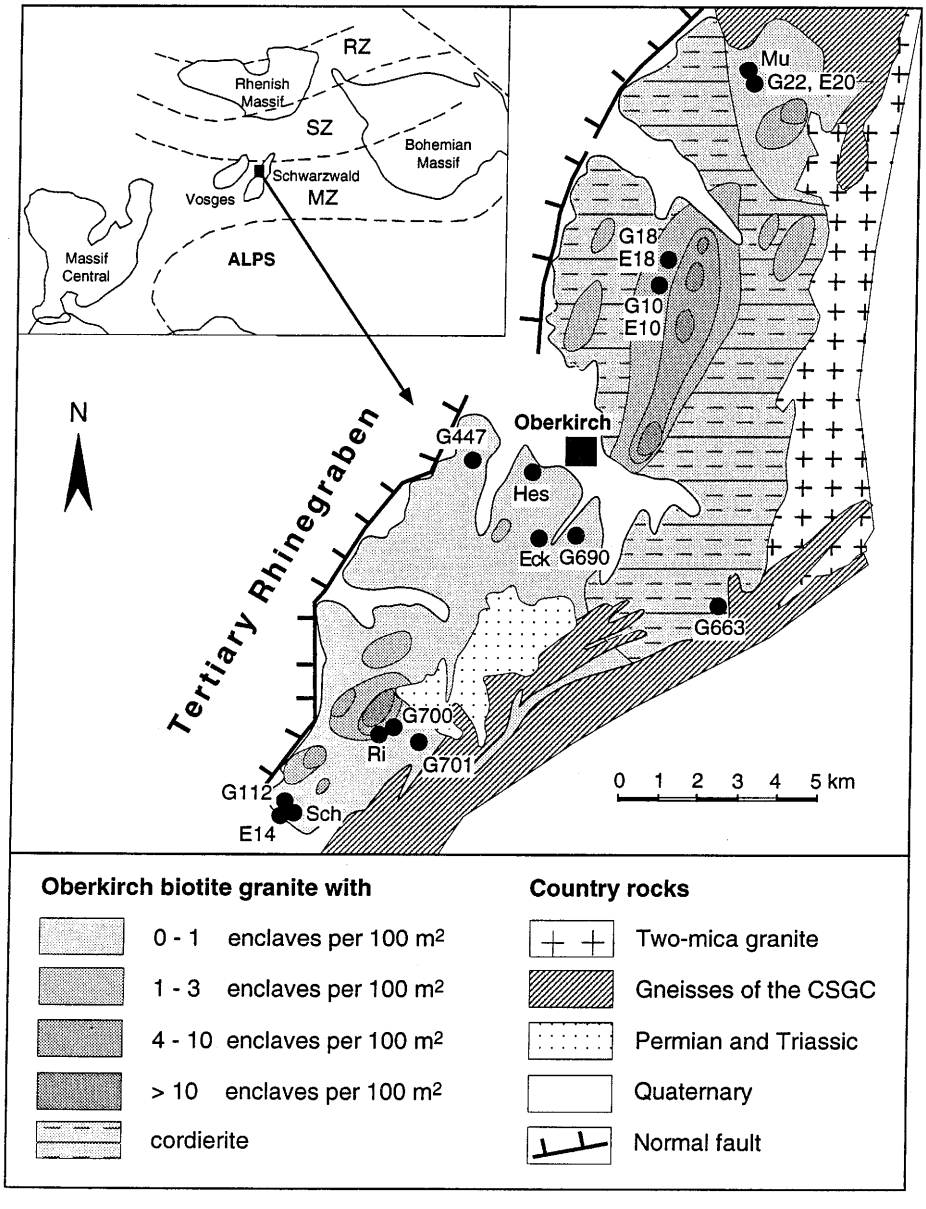

Fig. 1 Geological setting of the Oberkirch pluton and sample locations (*solid circles*). Frequency distribution of microgranular enclaves after Otto (1974). *Inset* shows location of the Oberkirch pluton within the central European Variscides. *RZ* Rhenohercynian zone; *SZ* Saxothuringian zone; *MZ* Moldanubian zone. (Kossmat 1927)

follows the regional structural pattern of the gneisses. Locally, the granite forms apophyses into the gneisses or it may contain large angular gneissic fragments. The contact itself is generally sharp and indicates the intrusive nature of the granite. The emplacement age can be constrained to 330 to 325 Ma as indicated by isotope dating on the high-grade metamorphic country rocks (e.g. U-Pb on monazites, Rb-Sr thin slab method on stromatic migmatites: Kalt et al. 1994a; K-Ar and Ar-Ar on hornblende: Lippolt et al. 1994; Rb-Sr on whole rock-biotite pairs: Von Drach 1978; Kalt et al. 1994b) as well as Rb-Sr and K-Ar ages on biotite from the Oberkirch granite itself (Faul and Jäger 1963; Von Drach 1978). In the east, the Oberkirch pluton and its country rocks were intruded by a two-mica granite (Fig. 1). During the Lower Permian, clastic sediments and felsic volcanics were deposited in small tectonic basins.

At the present level of erosion, most of the Oberkirch pluton comprises medium-grained biotite granite containing megacrysts of K-feldspar that locally show a weak flow orientation. The modes of the pluton are variable and increasing amounts of biotite and plagioclase are accompanied by decreasing amounts of quartz and K-feldspar (Table 1). The occurrence of cordierite is restricted to the central part of the exposed area (Fig. 1). Apart from the presence or absence of cordierite, no systematic compositional differences occur between the southern and central units of the pluton. The northern unit, however, is characterized by significantly greater amounts of biotite (Table 1). These regional variations in modal composition suggest that the pluton formed from at least three distinct granitic magma pulses. Contacts between the compositionally different units are, however, not exposed. Throughout the whole pluton, plagioclase crystals display normal core to rim zoning with only minor oscillations. Observed An contents range from 45 to 10 mol% and increase with the modal abundances of biotite and plagioclase. K-feldspar megacrysts have relatively large inclusion-free cores mantled by zones that contain oriented inclusions of plagioclase (An_{35} to An_{25}) and biotite. Beyond the essential minerals, apatite, zircon, allanite, magnetite and ilmenite are present as accessory phases.

Mafic microgranular enclaves are widespread throughout the pluton but are most abundant along a central, NNE-trending axis (Fig. 1). Their shapes are generally ovoid, although the larger ones are more variable. Textures and modes (Table 1) differ depending on the size of the enclaves. The most common, dm to m enclaves have dioritic to tonalitic compositions and display fine-grained doleritic textures. They contain subhedral elongate laths of plagioclase that show more or less continuous normal zoning (An_{70} to An_{26}). In addition, some enclaves (e.g. sample Eck1) contain rare plagioclase megacrysts that usually display discontinuous reverse zoning, with a corroded Ab-rich core (An_{37} to An_{25}) fringed by more calcic plagioclase that shows normal oscillatory zoning (An_{67} to An_{40}). Hornblende is present in all samples and shows subhedral to anhedral shapes. Approximately half of the microdioritic enclaves contain clinopyroxene which may be accompanied by traces of orthopyroxene. Both pyroxenes may be partially replaced by actinolitic hornblende. Another significant petrographic feature of these enclaves is the abundance of acicular apatite commonly

Table 1 Modes of representative samples from different rock types. Mineral abbreviations: *Px* clinopyroxene with subordinate amounts of orthopyroxene; *Hbl* hornblende; *Btt* biotite; *Kf* alkali feldspar; *Qtz* quartz; *Crd* cordierite; *Acc* accessory phases (magnetite, zircon, apatite, titanite)

Sample	Px	Hbl	Btt	Plag	Kf	Qtz	Crd	Acc
Hornblende-bearing microdioritic to microtonalitic enclaves (central parts)								
Mu1a	0.0	19.1	28.5	45.2	0.0	5.5	0.0	1.7
Mu2	0.0	23.1	19.0	52.7	0.0	3.6	0.0	1.6
Mu4	4.8	6.7	30.8	46.3	0.6	8.2	0.0	2.6
Mu5	6.1	0.3	29.8	44.0	1.0	17.4	0.0	1.4
Eck1	14.9	13.4	10.2	51.3	0.0	9.0	0.0	1.2
Sch1	8.6	16.2	11.8	58.8	0.0	3.1	0.0	1.5
Hes1	0.0	35.7	9.0	52.0	0.5	1.5	0.0	1.3
Hybrid granodioritic rims of microdioritic enclaves								
Sch3 (around Sch1)	1.0	4.6	17.3	38.7	16.5	21.0	0.0	0.9
Hes1a (around Hes1)	0.0	0.0	19.6	40.6	18.8	20.6	0.0	0.4
Hybrid tonalitic enclave (modified diorite)								
Eck2	0.0	4.8	23.5	42.7	7.6	20.5	0.0	0.9
Tonalitic enclaves								
E10g	0.0	0.0	26.3	44.5	1.5	27.2	0.0	0.5
E14/5	0.0	0.0	26.4	45.6	0.0	27.1	0.0	0.9
E14/6	0.0	0.0	46.3	34.9	0.0	18.3	0.0	0.5
E18k	0.0	0.0	33.9	37.3	1.7	26.3	0.0	0.8
E20d	0.0	0.0	27.0	49.0	0.0	23.0	0.0	1.0
Hybrid granodioritic enclaves								
E10sp	0.0	0.0	16.4	36.0	17.1	29.0	0.0	1.5
E18j	0.0	0.0	16.2	37.0	17.7	28.5	0.0	0.6
Synplutonic microdioritic dike (central part)								
Ri1	9.6	20.4	6.8	52.7	3.2	5.1	0.0	2.2
Cordierite-bearing granite								
G1	0.0	0.0	11.5	35.0	26.7	25.2	1.3	0.3
G10	0.0	0.0	9.8	36.6	25.1	26.0	2.1	0.4
G18	0.0	0.0	10.2	39.1	23.5	25.6	1.1	0.5
G663	0.0	0.0	9.8	34.7	22.8	30.9	1.5	0.3
Cordierite-free granite								
G22	0.0	0.0	16.4	40.1	21.1	22.0	0.0	0.4
G112	0.0	0.0	9.2	35.8	28.5	26.2	0.0	0.3
G447	0.0	0.0	12.1	29.9	30.0	27.7	0.0	0.3
G690	0.0	0.0	13.9	33.9	24.7	27.2	0.0	0.3
G700	0.0	0.0	10.6	37.1	24.8	27.3	0.0	0.2
G701	0.0	0.0	8.2	30.8	34.6	26.2	0.0	0.2

interpreted as evidence of undercooling (e.g. Wyllie et al. 1962; Vernon 1984, 1990). Additional accessory phases are titanite, magnetite, quartz and K-feldspar.

Many but not all dioritic enclaves are compositionally zoned, the rim being richer in quartz, K-feldspar and biotite, and the core in amphibole, pyroxenes and plagioclase. Textural relationships between the ferromagnesian minerals suggest partial replacement of clinopyroxene by hornblende, and of hornblende by biotite, preferably in the outer portions of enclaves. Plagioclase megacrysts with Ab-rich cores and normally zoned more An-rich mantles as well as quartz megacrysts are relatively abundant in the granodioritic rims. Some enclaves have been thoroughly modified resulting in a tonalitic to granodioritic composition with hornblende being (almost) completely replaced by biotite (e.g. samples Eck2, E20d).

Tonalitic and granodioritic enclaves containing biotite as the sole mafic mineral (Table 1) are less abundant and generally smaller (5–20 cm in diameter) than the microdioritic enclaves. Accessory phases include zircon, allanite, apatite, magnetite and ilmenite. Based on textural evidence, two end member types can be distinguished, namely: (1) fine-grained microtonalitic enclaves (e.g. samples E14/6, E14/5) that contain subhedral plagioclase grains showing continuous normal zoning (An_{47} to An_{20}) and variable amounts of plagioclase megacrysts. The megacrysts have relatively Ab-rich cores ($An_{29–20}$) overgrown by more An-rich normally zoned mantles (An_{40} to An_{26}). (2) Relatively coarse-grained, sometimes porphyritic enclaves of tonalitic to granodioritic compositions. These contain abundant megacrysts of plagioclase (Ab-rich cores jacketed by more An-rich normally-zoned mantles), quartz and K-feldspar.

In all types of enclave, K-feldspar megacrysts similar to those of the granite may be present, some lying across the contact between the enclave and granite host. In addition, some enclaves contain quartz megacrysts.

In the southern part of the pluton, diorites also occur as dike-like intrusive bodies measuring up to 6 m in width. The compositions and textures of these intrusive diorites are similar to those of the dioritic enclaves. A detailed study of the contact relationships between host granite and intrusive diorite bodies shows that dioritic magmas intruded into the almost solidified biotite granite. This results in the formation of a several centimeter- to decimeter-wide hybrid zone between diorite and granite. Fine-grained margins of the dioritic bodies suggest chilling against the colder granite. The latter was obviously infiltrated by dioritic melt along grain boundaries where granitic melt might have still existed. Mineral fragments from the granite (plagioclase, quartz, K-feldspar) are included in the marginal zones of the dioritic bodies. In these zones, hornblende and pyroxene are transformed to biotite.

Following these observations, Otto (1974) concluded that the mafic microgranular enclaves were derived from dioritic magma pulses that intruded the crystallizing granite and were thereby partially dismembered. Depending on the size of dismembered magma batches (globules) and the state of solidification of the granite magma, mingling and mixing of the contrasting magmas took place to variable degrees, producing either the tonalitic to granodioritic rims of larger microdioritic enclaves or isolated tonalitic to granodioritic enclaves of smaller size.

Apart from igneous-textured textured mafic enclaves, the granite contains xenoliths with metamorphic textures that show all stages of assimilation by the granitic magma (Otto 1974). These xenoliths are concentrated in the marginal parts of the pluton and most probably are derived from the metamorphic country rocks or equivalents thereof. More relictic xenoliths display angular or flattened shapes and have diameters of several centimeters, but some larger elongated gneiss fragments measuring up to several tens of meters in length were also found.

Analytical techniques

Major and trace (Ba, Nb, Zr, Y, Ni, and partly Rb and Sr) elements, were determined at the Mineralogisches Institut, University of Heidelberg, by standard wavelength-dispersive XRF techniques using lithium borate fusion disks and pressed powder pellets. Calibration was done with international reference samples. Abundances of Rb and Sr in most samples were determined by isotope dilution techniques (see below) and those of Cs, Th, U, Ta, Hf, Sc, and the rare earth elements (REE) were measured by instrumental neutron activation techniques at the Institut für Petrographie und Geochemie, University of Karlsruhe (Class et al. 1994). Rb-Sr isotope analyses were carried out at the Zentrallabor für Geochronologie (ZLG), University of Münster. For analytical details see Mezger et al. (1985) and Altherr et al. (1988).

All $^{87}Sr/^{86}Sr$ ratios are normalized to $^{86}Sr/^{88}Sr = 0.1194$ and are reported relative to a value of 0.71035 for the NBS SRM 987 Sr standard. Sm-Nd isotope analyses were done at the Bundesanstalt für Geowissenschaften und Rohstoffe, Hannover. Whole rock powders spiked with a $^{147}Sm/^{148}Nd$ tracer were dissolved in 120-ml screw-top Teflon PFA vials in a CEM microwave using a HF-HNO_3 acid mixture for 3–5 h. Sm and Nd were isolated in a first step using quartz glass columns filled with Dowex W-X8 (200–400 mesh) resin and in a second step using quartz glass columns containing Teflon powder coated with HDEHP (di(2-ethylhexyl)-orthophosphoric acid) as a cation exchange medium. Sm and Nd were measured as metals on Re filaments in static mode using a MAT 261 mass spectrometer equipped with five faraday collectors. Mass fractionation was corrected by normalizing to $^{146}Nd/^{144}Nd = 0.7219$ and to $^{154}Sm/^{149}Sm = 1.64609$ for Nd and Sm, respectively. Analytical precision was controlled by routine analysis of a SARM granite standard. Typical blank values for Sm and Nd were < 1 ng which in general is negligible in comparison with the element concentrations in the samples under investigation. $^{143}Nd/^{144}Nd$ ratios in Table 2 are given relative to $^{143}Nd/^{144}Nd = 0.511858$ for the La Jolla Nd standard. Two sigma errors for $^{143}Nd/^{144}Nd$ are estimated to be less than 0.000014. ε_{Nd} was calculated using $^{143}Nd/^{144}Nd = 0.512638$ and $^{147}Sm/^{144}Sm = 0.1967$ for CHUR.

Oxygen isotope analyses were performed by A. Matthews at The Hebrew University of Jerusalem (see Altherr et al. 1988 for analytical details) and at the Institut für Mineralogie, Petrologie und Geochemie, University of Tübingen. At Tübingen, oxygen was liberated from the whole rock samples by reaction with BrF_5 and subsequently converted to CO_2 by reaction with hot graphite (Clayton and Mayeda 1963). $^{18}O/^{16}O$ ratios were measured with a Finnigan MAT 252 mass spectrometer and are reported in the δ notation as per mil derivation from Standard Mean Ocean Water (SMOW). Results are considered precise to $\pm 0.2‰$. For inter-laboratory comparison, a value of $9.6 \pm 0.3‰$ was obtained for the NBS-28 quartz reference standard.

Whole rock geochemistry

Representative whole rock analyses are presented in Table 2. The data were plotted in variation diagrams with $Mg\# = [100 \times \text{molar } MgO/(MgO + 0.9\ FeO_{tot})]$ on the abscissa (Fig. 2), as in the mafic samples Mg# shows more variation than SiO_2. In most variation diagrams, the diorite samples (taken from the central parts of hornblende-bearing enclaves and from a synplutonic dike) form continuous trends. The abundances of TiO_2, P_2O_5, Na_2O, K_2O, Ba, Zr, Hf, Nb, Ta, Y and La, for example, all increase with decreasing Mg#, whereas those of Al_2O_3, CaO and Ni decrease. Except for Ba, Nb and La, the granitic host rocks do not follow the trends shown by the diorite samples but show a large scatter for most elements. No systematic differences were found between cordierite-bearing and cordierite-free samples. The sample G22 from the relatively mafic northern part of the pluton (Fig. 1) has an intermediate value of Mg# (40.0) compared to the whole range of values (49.1 to 36.6) shown by the other granite samples.

Table 2 Major [wt%] and trace element [ppm] abundances in representative samples from the Oberkirch pluton, Rock type abbreviations: *CDE* core of microdioritic enclave; *HTE* hybrid tonalitic enclave (modified diorite); *SDD* synplutonic dioritic dike; *TE* tonalitic enclave; *HDGr* samples from the hybrid zone between synplutonic dioritic dike Ri1 and granite GRi2; *HGdR* hybrid granodioritic rim around microdioritic enclave; *HGdE* hybrid granodioritic enclave; *CGr* cordierite-bearing granite; *Gr* granite free of cordierite. *ASI* = molar $Al_2O_3/(CaO + Na_2O + K_2O)$; *Mg#* = 100 × molar $MgO/(MgO + 0.9FeO_{tot})$. See text for analytical techniques

Sample	Hes1	Eck1	Ri1	Mu1a	Mu2	Mu4	Sch1	Mu5	Eck2	E10g
Rock type	CDE	CDE	SDD	CDE	CDE	CDE	CDE	CDE	HTE	TE
SiO_2	50.81	53.42	55.14	51.50	52.85	52.94	54.00	56.34	58.21	64.36
TiO_2	0.88	1.19	1.48	1.91	1.98	2.13	2.21	2.05	1.65	0.73
Al_2O_3	17.25	17.26	17.04	16.70	16.66	16.34	15.80	16.35	15.90	15.75
Fe_2O_3	1.46	1.80	1.42	1.40	1.26	1.39	2.35	1.18	2.18	1.50
FeO	8.36	6.75	6.20	8.47	8.30	7.95	8.34	7.27	6.03	4.52
MnO	0.17	0.14	0.12	0.16	0.14	0.15	0.20	0.14	0.13	0.08
MgO	8.24	6.27	4.61	5.32	4.48	4.40	4.38	2.89	2.94	2.56
CaO	5.90	6.90	6.07	6.46	6.40	5.90	5.70	5.29	4.12	2.38
Na_2O	2.90	2.98	3.21	2.81	3.50	3.33	3.11	3.51	3.30	3.53
K_2O	1.50	1.62	1.84	2.88	2.43	3.14	1.77	3.11	3.34	2.85
P_2O5	0.11	0.16	0.33	0.34	0.37	0.33	0.41	0.47	0.47	0.23
H_2O	2.60	1.88	2.66	1.62	1.65	1.72	2.02	1.25	1.77	1.33
Total	100.18	100.37	100.12	99.57	100.02	99.72	100.29	99.85	100.04	99.82
Mg#	62.8	59.7	55.0	52.0	48.5	48.6	45.3	40.7	42.1	46.3
ASI	1.01	0.90	0.93	0.86	0.83	0.83	0.91	0.87	0.96	1.19
Cr	211	280	196	95	103	130	138	173	181	168
Ni	138	47	35	48	32	27	29	13	19	44
Sc	15.2	23.7	21.0	19.9	19.3	20.8	22.5	21.4	20.8	11.1
Cs	17.5	6.6	26.2	8.5	5.9	8.1	12.0	6.2	8.9	15.3
Rb	79	68	71	175	98	136	114	133	148	254
Sr	285	345	388	345	379	401	325	338	306	153
Ba	317	363	854	481	623	782	578	971	624	415
Zr	99	116	238	215	238	171	205	286	203	238
Hf	2.11	2.96	5.84	5.34	5.59	5.64	4.87	6.65	5.49	5.72
Nb	5	4	7	6	9	7	10	12	10	10
Ta	0.52	0.75	0.98	1.04	1.56	1.23	1.42	1.92	1.39	1.68
Th	4.2	4.6	12.9	10.6	7.7	11.4	6.4	11.7	10.9	19.4
U	1.2	1.2	2.5	3.3	2.0	2.5	3.2	1.9	2.9	4.6
Y	21	27	31	32	31	29	36	32	36	21
La	19.9	26.8	48.2	38.1	35.3	45.1	40.2	57.0	47.4	57.4
Ce	37.9	48.5	89.1	75.0	67.5	89.2	76.7	107.0	84.5	91.7
Nd	18.7	22.4	42.8	37.5	35.7	44.3	36.0	49.0	43.8	43.3
Sm	3.97	5.02	8.01	7.84	7.66	8.88	8.64	9.28	8.90	6.86
Eu	1.35	1.82	1.85	1.92	2.19	2.19	2.35	1.98	1.96	0.96
Gd	4.2	5.4	6.8	7.1	7.5	7.4	9.2	8.2	8.9	5.1
Tb	0.66	0.85	0.96	1.02	1.14	1.10	1.50	1.13	1.28	0.70
Ho	0.84	1.16	n.a.	1.36	1.21	1.19	1.84	1.43	1.64	0.85
Tm	0.32	0.47	0.43	0.55	0.50	0.47	0.69	0.43	0.62	0.32
Yb	2.05	3.00	2.88	3.37	3.12	3.16	3.82	2.53	3.88	2.15
Lu	0.30	0.42	0.41	0.46	0.47	0.48	0.54	0.33	0.52	0.31

Sample	E14/5	E14/6	E20d	E18k	Ri4	Ri8	Hes1a	Sch3	E10sp	E18j
Rock type	TE	TE	TE	TE	HDGr	HDGr	HGdR	HGdR	HGdE	HGdE
SiO_2	64.05	53.70	61.00	63.00	58.14	68.51	66.19	61.70	67.25	65.90
TiO_2	1.03	1.40	1.45	0.82	1.44	0.56	0.68	1.13	0.67	0.70
Al_2O_3	15.37	16.86	16.39	16.00	16.17	14.74	15.59	16.10	15.18	15.13
Fe_2O_3	1.08	1.56	1.84	1.59	2.68	1.00	0.66	1.09	0.89	1.12
FeO	4.65	6.71	5.01	4.97	4.49	2.63	3.56	4.57	3.35	3.72
MnO	0.08	0.13	0.07	0.08	0.08	0.04	0.06	0.08	0.06	0.06
MgO	3.33	6.39	2.26	3.08	3.54	1.27	1.35	1.68	1.76	1.89
CaO	2.09	3.09	3.54	2.54	5.03	1.28	1.86	3.91	1.75	1.86
Na_2O	3.22	2.98	3.71	3.22	3.17	3.59	3.98	3.31	3.29	3.11
K_2O	2.63	3.29	2.54	2.98	2.96	4.22	3.73	4.15	3.96	4.35
P_2O5	0.21	0.21	0.48	0.07	0.35	0.17	0.30	0.34	0.23	0.24
H_2O	2.07	3.77	1.19	1.52	1.81	1.38	1.45	1.47	1.20	1.27
Total	99.81	100.08	99.48	99.87	99.86	99.39	99.41	99.53	99.59	99.35
Mg#	54.0	60.9	40.2	48.8	50.4	41.6	39.2	37.5	45.6	44.2
ASI	1.29	1.20	1.07	1.22	0.92	1.15	1.12	0.94	1.18	1.15
Cr	n.a.	537	268	240	146	n.a.	n.a.	72	70	n.a.
Ni	17	31	15	39	14	20	11	11	13	22
Sc	16.9	27.2	17.0	n.a.	19.2	21.0	11.0	13.6	10.3	10.8

Table 2 (Contd.)

Sample Rock type	E1415 TE	E1416 TE	E20d TE	E18k TE	Ri4 HDGr	Ri8 HDGr	Hes1a HGdR	Sch3 HGdR	E10sp HGdE	E18j HGdE
Cs	22.3	23.3	19.2	n.a.	20.3	26.2	14.6	10.7	15.0	9.6
Rb	222	214	257	229	120	71	170	184	229	217
Sr	129	143	246	184	332	388	176	337	132	259
Ba	407	537	795	378	877	824	794	965	343	450
Zr	188	180	322	228	263	238	270	235	189	191
Hf	4.12	4.16	9.08	n.a.	6.03	5.84	7.53	6.19	4.38	5.71
Nb	8	6	15	10	9	7	11	10	11	10
Ta	1.50	0.79	1.45	n.a.	1.12	0.98	1.50	1.58	2.33	1.45
Th	17.4	8.5	21.8	n.a.	14.0	12.9	23.1	15.4	17.5	20.3
U	6.8	8.0	4.1	n.a.	3.5	2.5	4.2	5.8	3.5	7.8
Y	22	26	32	22	33	31	31	31	23	24
La	34.0	28.1	58.9	n.a.	66.2	46.6	55.5	61.0	43.2	52.4
Ce	62.4	57.4	123.5	n.a.	117.5	86.2	97.8	110.7	76.8	96.1
Nd	30.7	31.0	53.5	n.a.	47.7	41.3	44.3	48.7	35.8	42.2
Sm	6.27	6.82	10.35	n.a.	10.10	7.74	8.26	9.94	6.68	7.40
Eu	1.03	1.08	1.90	n.a.	2.20	1.79	1.06	1.92	0.76	1.11
Gd	5.8	5.9	8.8	n.a.	9.6	6.6	6.5	8.8	4.6	5.7
Tb	0.79	0.88	1.26	n.a.	1.34	0.93	0.90	1.19	0.74	0.84
Ho	0.94	1.13	n.a.	n.a.	1.78	n.a.	0.97	1.39	0.84	1.12
Tm	0.40	0.45	0.48	n.a.	0.55	0.40	0.33	0.59	0.37	0.42
Yb	2.40	2.93	2.95	n.a.	3.55	2.78	2.10	3.18	2.15	2.35
Lu	0.33	0.44	0.39	n.a.	0.47	0.37	0.28	0.44	0.31	0.34

Sample Rock type	G10 CGr	G18 CGr	G663 CGr	G1 CGr	G112 Gr	G22 Gr	G447 Gr	G690 Gr	G700 Gr	G701 Gr	GRi2 Gr
SiO_2	68.86	68.39	70.10	70.32	70.02	63.31	70.38	67.77	70.32	68.53	69.44
TiO_2	0.50	0.57	0.46	0.35	0.34	0.89	0.43	0.62	0.36	0.43	0.45
Al_2O_3	14.95	15.25	14.22	14.63	14.70	16.45	14.46	14.95	14.60	15.33	14.85
Fe_2O_3	0.89	0.30	0.51	0.63	0.32	0.41	0.46	0.73	0.74	0.77	1.09
FeO	2.30	3.16	2.43	2.10	2.25	4.26	2.14	2.81	1.92	2.30	2.01
MnO	0.06	0.06	0.05	0.04	0.04	0.06	0.05	0.06	0.04	0.04	0.03
MgO	1.32	1.68	1.41	0.78	0.74	1.56	0.85	1.45	0.76	0.88	1.00
CaO	1.45	1.53	1.11	0.67	1.05	2.79	1.06	1.53	0.67	1.46	1.13
Na_2O	3.12	3.18	2.76	3.58	3.38	3.46	3.09	3.30	3.60	3.26	3.40
K_2O	4.64	4.42	4.59	4.77	5.07	4.68	5.37	4.85	4.76	5.13	4.67
P_2O5	0.21	0.24	0.21	0.22	0.17	0.33	0.18	0.23	0.24	0.21	0.22
H_2O	1.15	1.27	1.60	1.21	0.97	1.00	0.99	1.36	1.31	1.02	1.03
Total	99.45	100.05	99.45	99.30	99.05	99.20	99.46	99.66	99.32	99.36	99.32
Mg#	45.7	49.2	49.1	36.7	36.6	40.0	39.7	45.3	36.8	36.8	39.8
ASI	1.17	1.19	1.23	1.19	1.13	1.04	1.13	1.11	1.19	1.13	1.17
Cr	n.a.	42	n.a.	11	n.a.	34	n.a.	n.a.	n.a.	13	n.a.
Ni	15	16	16	13	10	13	11	12	9	10	9
Sc	8.1	9.1	7.3	6.0	6.7	11.5	7.0	8.4	6.1	7.7	6.5
Cs	14.1	15.7	24.3	16.4	16.9	9.0	20.7	15.4	16.6	19.7	17.0
Rb	219	211	238	208	204	212	269	225	206	206	207
Sr	243	263	134	148	143	246	107	155	148	153	133
Ba	670	666	429	790	945	1050	578	727	819	1040	843
Zr	170	182	173	187	181	283	170	214	183	227	182
Hf	4.87	5.52	4.58	4.96	5.02	7.84	4.73	5.35	4.68	5.63	4.76
Nb	9	9	9	8	8	14	9	10	10	10	10
Ta	1.73	2.01	2.03	1.33	1.63	1.58	2.12	1.63	2.19	1.80	1.87
Th	19.8	21.4	20.6	16.8	22.0	27.3	21.9	21.7	17.2	20.1	17.4
U	9.9	12.5	4.2	4.8	4.7	3.6	5.4	4.4	4.8	4.7	5.9
Y	23	25	22	26	29	25	28	27	23	28	25
La	61.5	58.1	47.7	65.3	42.8	73.3	47.6	52.6	73.4	52.7	58.3
Ce	112.1	104.9	85.3	95.3	77.8	131.8	90.7	92.9	118.3	92.0	104.0
Nd	45.7	44.0	38.2	43.5	31.6	55.5	38.3	39.0	51.9	37.9	45.4
Sm	8.23	7.81	7.09	8.73	6.39	10.16	7.60	7.49	10.10	7.15	8.34
Eu	1.25	1.16	0.87	1.09	0.81	1.50	0.91	1.04	1.28	1.09	1.16
Gd	7.0	5.1	5.3	6.3	5.5	8.8	6.3	5.5	8.9	5.2	7.3
Tb	1.00	0.84	0.72	0.89	0.88	1.00	0.97	0.85	1.12	0.86	1.03
Ho	1.28	1.20	0.97	0.77	1.20	1.05	1.30	n.a.	n.a.	0.80	1.33
Tm	0.42	0.41	0.34	0.26	0.42	0.30	0.51	0.40	0.31	0.31	0.40
Yb	2.55	2.19	1.95	1.46	2.28	1.76	3.09	2.23	1.79	1.89	2.50
Lu	0.35	0.34	0.26	0.22	0.31	0.21	0.44	0.29	0.24	0.26	0.35

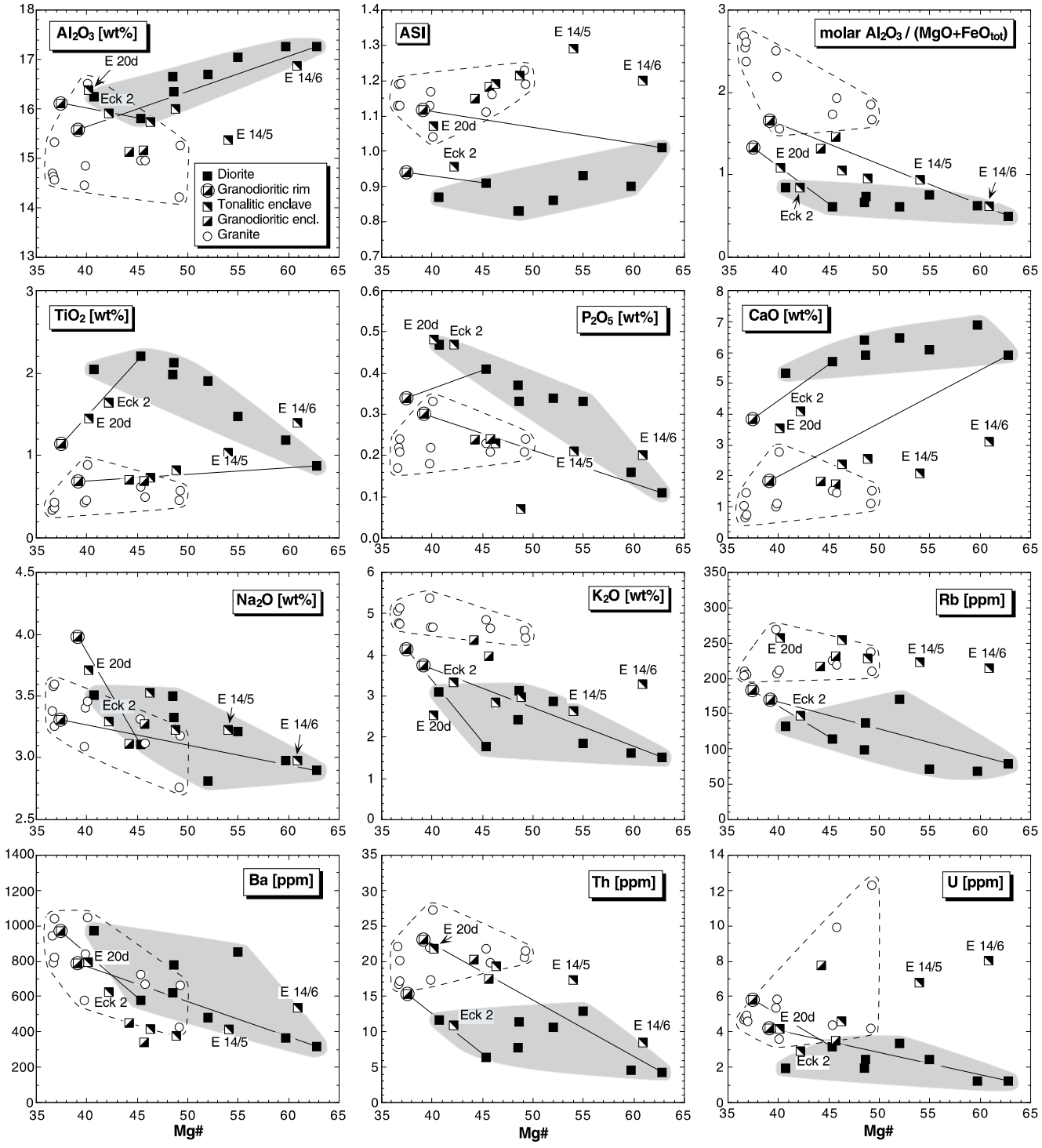

Fig. 2 Variation of element abundances and some element ratios with Mg# = [100 × molar MgO/(MgO + 0.9 FeO_{tot})] in samples from the composite Oberkirch pluton. *ASI* Molar ratio of Al_2O_3/($CaO + Na_2O + K_2O$). Enclave core-rim pairs are marked by tie lines. Tonalitic samples Eck2 and E20d represent thoroughly modified diorites with hornblende being (almost) completely replaced by biotite aggregates. Samples E14/6 and E14/5 were taken from fine-grained microtonalitic enclave cores

Samples from the granodioritic rims of zoned enclaves plot within or near the compositional fields defined by the granite samples (Fig. 2). Their compositions are, however, different from those of granodioritic enclaves that show no evidence of formerly existing hornblende. This is particularly evident in the variation diagrams for Al_2O_3, P_2O_5, Rb, Ba and Y. Tonalitic enclaves show a large spread in their chemical compositions. Samples Eck2 and E20d, representing modified dioritic enclaves, have compositions that are intermediate between those of the diorites and the granodioritic

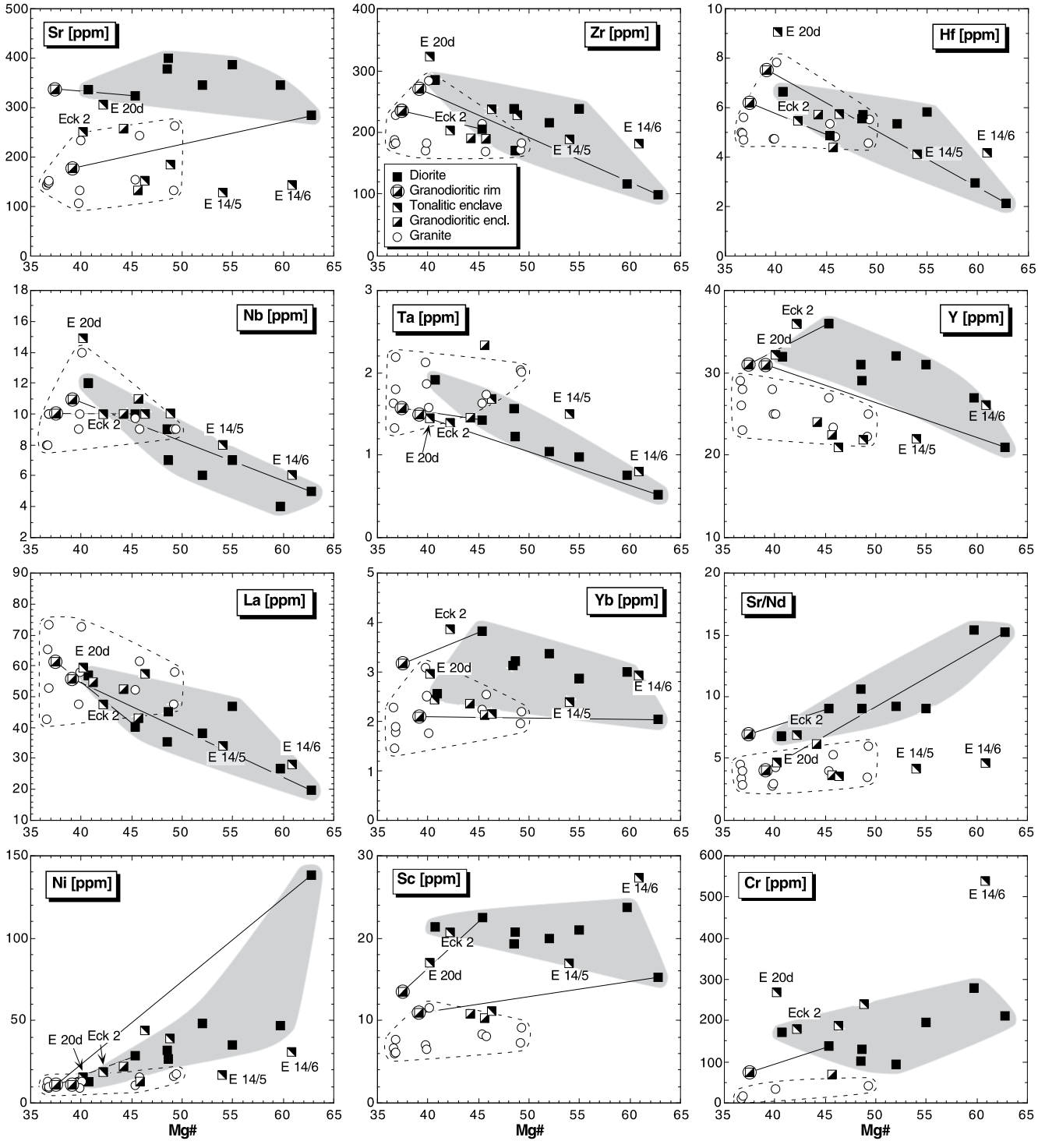

Fig. 2 Continued

rims of zoned enclaves. On the other hand, the samples E14/6 and E14/5 are compositionally different from both granites and diorites. Compared with the latter, they are, for example, characterized by higher values of ASI = [molar $Al_2O_3/(CaO + Na_2O + K_2O)$], lower abundances of CaO, Sr, Ni and higher abundances of Rb, U and Cr (Fig. 2).

Chondrite-normalized (cn) REE patterns of representative samples are shown in Fig. 3. In the figure, the data have been arranged such that patterns of mafic enclaves are combined with those of their granitic hosts. All granite samples (Fig. 3a) show pronounced negative Eu anomalies ($Eu/Eu^* = Eu_{cn}/(Sm_{cn} \times Gd_{cn})^{0.5} = 0.57$ to 0.41). Fractionation of the medium REE (MREE) over the heavy REE (HREE) is highly variable with $(Tb/Yb)_{cn}$ values ranging from 1.33 to 2.65 (Figs. 4a, d–i, k).

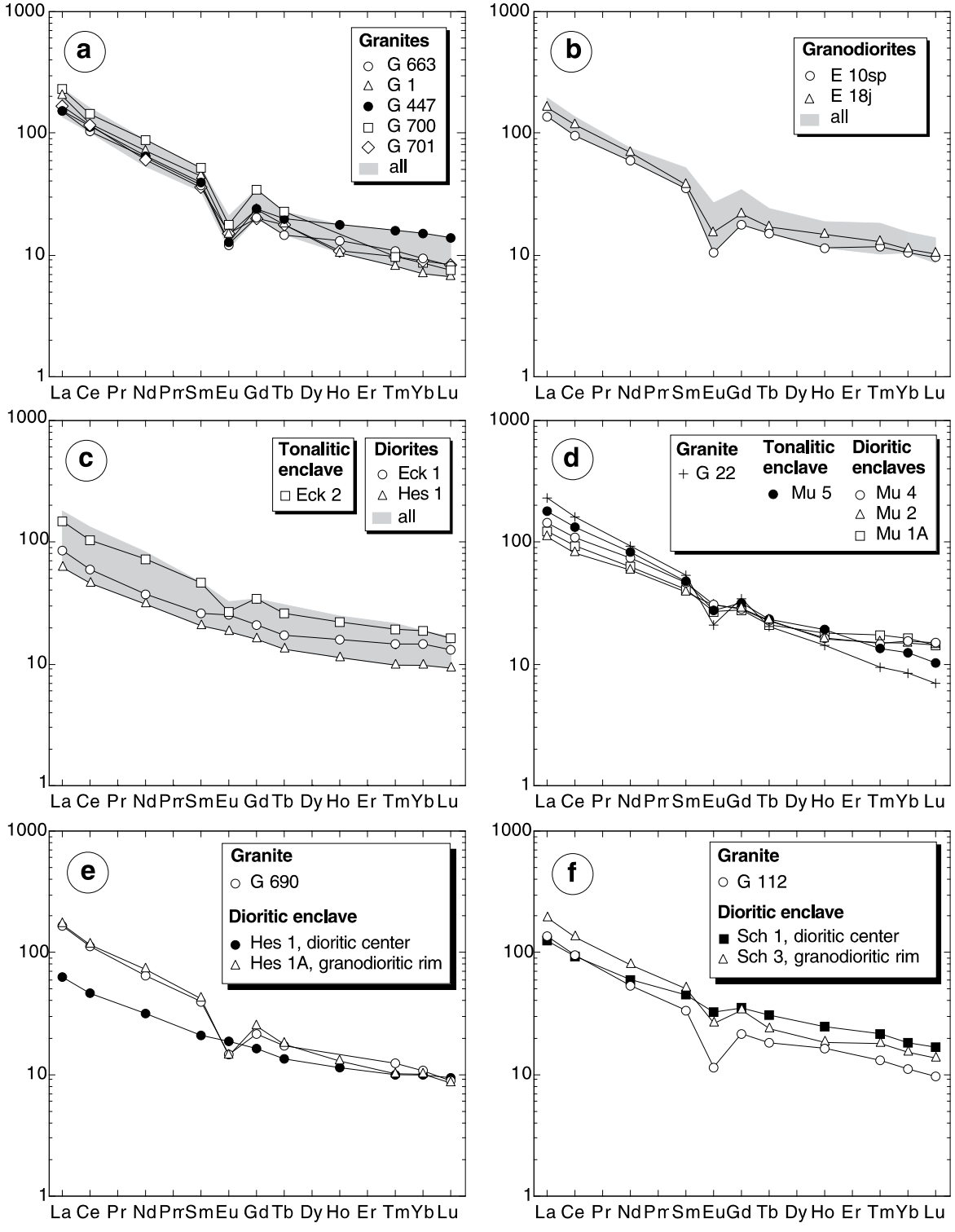

Fig. 3a–k Chondrite-normalized rare earth element abundance patterns [normalized to values given in Boynton (1984)] for representative samples of the different rock types

REE patterns of granodiorites (Fig. 4b, e, f) are characterized by pronounced negative Eu anomalies (Eu/Eu* = 0.63 to 0.42) and low $(Tb/Yb)_{cn}$ values (1.46 to 1.81). The diorites show variable REE patterns (Fig. 4c, d) and the Eu/Eu* values tend to decrease (not shown), while the abundances of the REE tend to increase with decreasing Mg# (Fig. 2). $(Tb/Yb)_{cn}$ values are generally low (1.20–1.89). Most tonalitic and granodioritic enclaves have REE patterns that are similar to those of their granitic hosts (e.g. Fig. 4e, g–i).

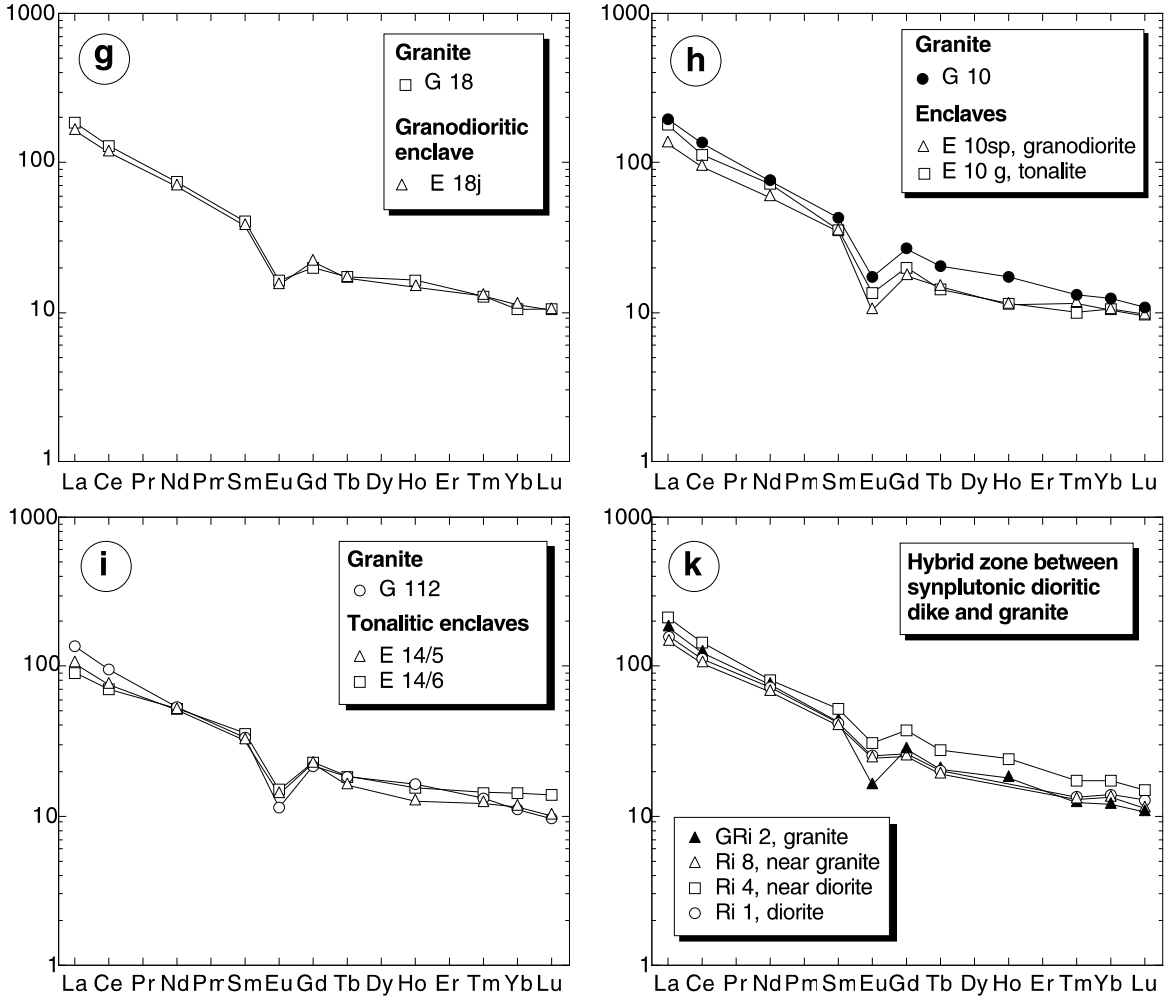

Fig. 3 Continued

Isotopes

Nd, Sr and O isotope data are given in Table 3 and presented in Fig. 4. Measured Nd and Sr isotope ratios have been recalculated to 325 Ma, a date corresponding to the Rb-Sr and K-Ar ages on biotite (Faul and Jäger 1963; Von Drach 1978) and thought to be a good approximation for the intrusion age (I). $\varepsilon_{Nd}(I)$ values and $^{87}Sr/^{86}Sr(I)$ values of bulk rock samples range from −1.2 to −6.8 and from 0.70549 to 0.71058, respectively, whereby the data show a large scatter (Fig. 4a). Neglecting granite sample G447, which shows an exceptionally low $^{87}Sr/^{86}Sr(I)$ value (possibly due to loss of radiogenic Sr; Table 3), calculated initial Sr isotope ratios for the granites are higher than those for diorites and there is little overlap in $\varepsilon_{Nd}(I)$ values for both rock groups. $\delta^{18}O$ values of the granites range from 9.9 to 11.9% and are significantly higher than those of diorites (Fig. 5b, c). Two diorite samples (Ri1 and Hes1) bearing petrographic evidence for hydrothermal alteration, such as formation of secondary sericite and hematite in plagioclase, of talc and serpentine from orthopyroxene and of chlorite from biotite, yielded relatively low $\delta^{18}O$ values (5.4 and 5.0‰, respectively).

Whereas the isotopic characteristics of granodiorites are similar to those of the granites, tonalitic enclaves show highly variable isotopic signatures. Samples Eck2 and E20d, which originated from diorites by hybridization processes, show Nd-Sr characteristics that are intermediate between those of the diorites and those of the granites and differ from those of the microtonalitic enclaves represented by samples E14/5 and E14/6 (Fig. 4a).

In zoned enclaves, granodioritic rims have lower $\varepsilon_{Nd}(I)$ and higher $^{87}Sr/^{86}Sr(I)$ values than dioritic cores (Fig. 4a). Rb-Sr isotope relationships of intrusive diorite Ri1, host granite GRi2 and the two samples from the hybrid zone between granite and diorite (samples Ri4 and Ri8) are roughly in accordance with a mingling and mixing relationship between the slightly older, almost solidified granite and the younger intrusive diorite as suggested by textural evidence (Fig. 4d). In addition to whole rock aliquots, handpicked plagioclase concentrates from three samples (granite G10, microtonalitic enclave E14/6, synplutonic dioritic dike Ri1) were analyzed for Rb and Sr isotope ratios. Whereas plagioclase

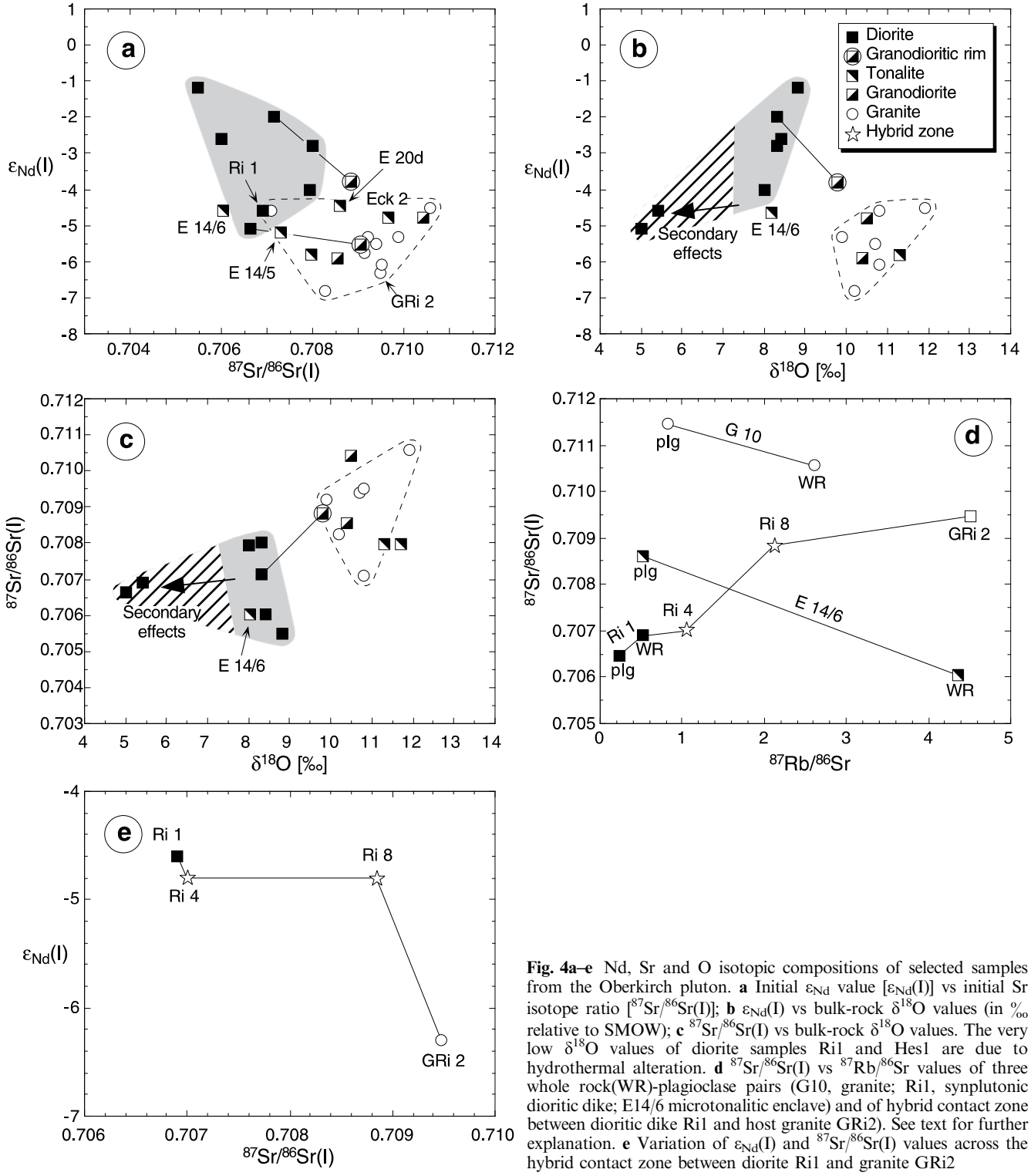

Fig. 4a–e Nd, Sr and O isotopic compositions of selected samples from the Oberkirch pluton. **a** Initial ε_{Nd} value [$\varepsilon_{Nd}(I)$] vs initial Sr isotope ratio [$^{87}Sr/^{86}Sr(I)$]; **b** $\varepsilon_{Nd}(I)$ vs bulk-rock $\delta^{18}O$ values (in ‰ relative to SMOW); **c** $^{87}Sr/^{86}Sr(I)$ vs bulk-rock $\delta^{18}O$ values. The very low $\delta^{18}O$ values of diorite samples Ri1 and Hes1 are due to hydrothermal alteration. **d** $^{87}Sr/^{86}Sr(I)$ vs $^{87}Rb/^{86}Sr$ values of three whole rock(WR)-plagioclase pairs (G10, granite; Ri1, synplutonic dioritic dike; E14/6 microtonalitic enclave) and of hybrid contact zone between dioritic dike Ri1 and host granite GRi2). See text for further explanation. **e** Variation of $\varepsilon_{Nd}(I)$ and $^{87}Sr/^{86}Sr(I)$ values across the hybrid contact zone between diorite Ri1 and granite GRi2

concentrates from samples G10 and E14/6 exhibit $^{87}Sr/^{86}Sr(I)$ values that are significantly higher than those of the respective whole rock aliquots, the calculated $^{87}Sr/^{86}Sr(I)$ value for the plagioclase concentrate from sample Ri1 is slightly lower than that of the whole rock (Table 3, Fig. 4d). The difference between the calculated $^{87}Sr/^{86}Sr(I)$ values for the plagioclase concentrate and whole rock is, however, regarded as insignificant, since small amounts of secondary sericite, if present in the plagioclase concentrate of sample Ri1, will most probably result in a slightly elevated Rb/Sr ratio and a lower $^{87}Sr/^{86}Sr(I)$ value.

Table 3 Sm-Nd, Rb-Sr and O isotope data for Oberkirch granitoids. Initial ε_{Nd} values [$\varepsilon_{Nd}(I)$] and initial Sr isotope ratios [$^{87}Sr/^{86}Sr(I)$] are based on 325 Ma. $\delta^{18}O$ values are relative to SMOW; values given in parantheses are thought to be due to hydrothermal alteration

Sample	Sm [ppm]	Nd [ppm]	$^{147}Sm/^{144}Nd$	$^{143}Nd/^{144}Nd$	$\varepsilon_{Nd}(I)$	$^{87}Rb/^{86}Sr$	$^{87}Sr/^{86}Sr$	$^{87}Sr/^{86}Sr(I)$	$\delta^{18}O$ [‰]
Hornblende-bearing microdioritic to microtonalitic enclaves (central parts)									
Hes1	4.19	18.69	0.1349	0.512248	−5.1	0.801	0.71035(2)	0.70664	[5.0]
Eck1	5.03	21.73	0.1393	0.512309	−4.0	0.572	0.71059(3)	0.70794	8.0
Mu1a	7.72	37.73	0.1232	0.512422	−1.2	1.464	0.71226(3)	0.70549	8.8
Mu2	7.63	36.07	0.1273	0.512359	−2.6	0.751	0.70948(8)	0.70601	8.4
Mu4	8.55	46.05	0.1118	0.512313	−2.8	0.985	0.71257(4)	0.70801	8.3
Sch1	8.33	37.88	0.1324	0.512401	−2.0	1.010	0.71182(4)	0.70715	8.3
Mu5						1.139	0.71312(5)	0.70785	
Hybrid tonalitic enclave									
Eck2	9.13	43.29	0.1270	0.512244	−4.8	1.397	0.71612(3)	0.70966	
Hybrid granodioritic rims of microdioritic enclaves									
Hes1a	8.54	43.44	0.1184	0.512183	−5.6	2.795	0.72199(2)	0.70906	
Sch3	9.61	50.55	0.1145	0.512267	−3.8	1.590	0.71617(4)	0.70882	9.8
Tonalitic enclaves									
E10g	7.66	46.52	0.0992	0.512135	−5.8	4.823	0.73028(6)	0.70797	11.3
E14/5	6.25	30.95	0.1216	0.512210	−5.2	4.980	0.73035(6)	0.70731	
E14/6	7.05	31.66	0.1340	0.512271	−4.6	4.354	0.72618(3)	0.70604	8.1
E14/6 plg						0.527	0.71105(4)	0.70861	
E18k						3.599	0.72462(4)	0.70797	11.7
E20d	10.55	53.86	0.1180	0.512243	−4.4	3.027	0.72260(3)	0.70860	
Hybrid granodioritic enclaves									
E10sp	6.90	36.13	0.1151	0.512161	−5.9	5.052	0.73193(4)	0.70856	10.4
E18j	7.59	42.21	0.1083	0.512204	−4.8	2.429	0.72166(4)	0.71042	10.5
Synplutonic dioritic dike									
Ri1	8.94	47.47	0.1134	0.512227	−4.6	0.530	0.70935(2)	0.70690	[5.4]
Ri1, plg						0.242	0.70759(6)	0.70647	
Hybrid zone between synplutonic dioritic dike Ri1 and granite GRi2									
Ri4	9.72	51.27	0.1142	0.512219	−4.8	1.049	0.71185(2)	0.70700	
Ri8	8.00	44.14	0.1091	0.512204	−4.8	2.127	0.71868(3)	0.70884	
Cordierite-bearing granite									
G1	8.85	47.68	0.1118	0.512185	−5.3	4.072	0.72873(4)	0.70989	
G10(1)	7.89	44.63	0.1065	0.512216	−4.5	2.610	0.72265(3)	0.71058	11.9
G10(2)	8.13	46.20	0.1060	0.512208	−4.6				
G10, plg						0.825	0.71528(5)	0.71146	
G18						2.321	0.72079(2)	0.71005	11.9
G663	6.94	38.19	0.1094	0.512105	−6.8	5.164	0.73215(6)	0.70826	10.2
Cordierite-free granite									
G22	10.12	57.60	0.1058	0.512175	−5.3	2.494	0.72074(6)	0.70920	9.9
G112	6.20	30.88	0.1209	0.512196	−5.5	4.166	0.72866(6)	0.70939	10.7
G447	7.54	38.85	0.1168	0.512232	−4.6	7.299	0.74084(2)	0.70708	10.8
G690	7.31	37.7	0.1167	0.512176	−5.7	4.203	0.72857(2)	0.70913	
G700	9.68	52.57	0.1109	0.512172	−5.5				
G701	7.25	38.40	0.1137	0.512149	−6.1	3.899	0.72750(5)	0.70950	10.8
GRi2	8.11	42.86	0.1139	0.512140	−6.3	4.517	0.73036(4)	0.70947	

Discussion

Origin of granitic magma

Granite samples display large and nonsystematic compositional variations (Figs. 3, 5) that cannot be explained by simple processes such as fractional crystallization or binary magma mixing alone. Instead, processes such as (1) partial melting of a heterogeneous source without subsequent homogenization, (2) multiple intrusion of compositionally different magmas with subsequent mingling and mixing or (3) assimilation and fractional crystallization (AFC), involving a (mantle-derived) mafic melt and a heterogeneous crustal assimilant, have to be envisaged. Isotopic signatures, such as low $\varepsilon_{Nd}(I)$ values in combination with high $^{87}Sr/^{86}Sr(I)$ and $\delta^{18}O$ values (Fig. 4) do not suggest a contribution from mantle-derived melts but allow for a purely crustal origin.

Compositional differences of magmas produced by partial melting of different source rocks under variable melting conditions may best be visualized in terms of molar oxide ratios, such as K_2O/Na_2O, $Al_2O_3/(MgO + FeO_{tot})$ and $CaO/(MgO + FeO_{tot})$. Partial

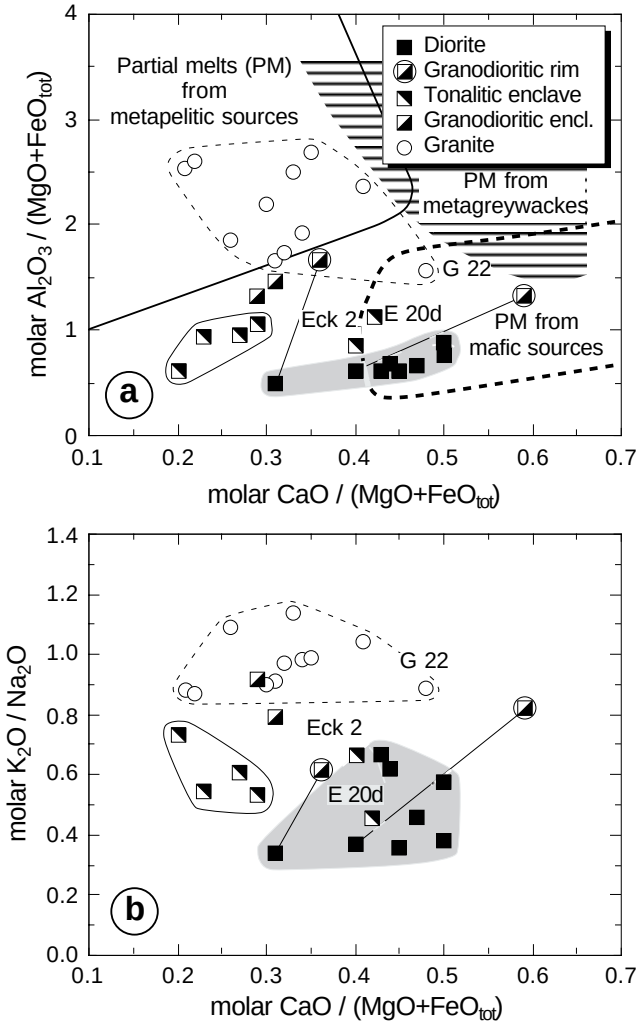

Fig. 5a–b Chemical compositions of different rock types from the Oberkirch pluton. **a** Molar $Al_2O_3/(MgO + FeO_{tot})$ vs molar $CaO/(MgO + FeO_{tot})$. *Outlined fields* denote compositions of partial melts obtained in numerous experimental studies by dehydration melting of various bulk compositions (data sources: Conrad et al. 1988; Le Breton and Thompson 1988; Vielzeuf and Holloway 1988; Carroll and Wyllie 1990; Beard and Lofgren 1991; Patiño Dource and Johnston 1991; Rapp et al. 1991; Rushmer 1991; Winther and Newton 1991; Wolf and Wyllie 1991, 1994; Skjerlie et al. 1993; Beard et al. 1994; Sen and Dunn 1994; Skjerlie and Johnston 1994, 1996; Vielzeuf and Montel 1994; Gardien et al. 1995; Patiño Douce and Beard 1995, 1996; Rapp 1995; Rapp and Watson 1995; Patiño Douce 1996; Singh and Johannes 1996; Thompson 1996; Winther 1996). **b** Molar K_2O/Na_2O vs molar $CaO/(MgO + FeO_{tot})$. Core-rim pairs from zoned enclaves are marked by tie lines. Samples Eck2 and E20d were formed by hybridization from former diorites. See text for further explanation

melts derived from mafic meta-igneous sources, for example, have lower values of $Al_2O_3/(MgO + FeO_{tot})$ and K_2O/Na_2O, but higher values of $CaO/(MgO + FeO_{tot})$ than partial melts derived from metapelites (compare, for example, data given in Conrad et al. 1988; Le Breton and Thompson 1988; Vielzeuf and Holloway 1988; Carroll and Wyllie 1990; Beard and Lofgren 1991; Patiño Dource and Johnston 1991; Rapp et al. 1991; Rushmer 1991; Winther and Newton 1991; Wolf and Wyllie 1991, 1994; Skjerlie et al. 1993; Beard et al. 1994; Sen and Dunn 1994; Skjerlie and Johnston 1994, 1996; Vielzeuf and Montel 1994; Gardien et al. 1995; Rapp 1995; Rapp and Watson 1995; Patiño Douce and Beard 1995, 1996; Patiño Douce 1996; Singh and Johannes 1996; Thompson 1996; Winther 1996). As can be seen from Fig. 5, the granite samples have higher values of $Al_2O_3/(MgO + FeO_{total})$ and K_2O/Na_2O than the enclaves. These characteristics, in combination with relatively low CaO/(MgO + FeOtot) values, suggest that the granitic magmas were derived from metapelitic source rocks. Such an origin is compatible with the peraluminous nature of the granite samples as reflected by high ASI values (1.04–1.19; Table 2 and Fig. 2) and the widespread occurrence of cordierite (Fig. 1). Significant negative Eu anomalies in REE_{cn} patterns (Fig. 3) as well as variable $(Tb/Yb)_{cn}$ values ranging from 1.33 to 2.65 may imply a heterogeneous source with variable amounts of feldspar and garnet. The role of garnet as a restite phase is also reflected by relatively low abundances of HREE (e.g. Yb), Sc and Y (Fig. 2).

Strong evidence for the assimilation of crustal material into the ascending granitic magma is provided by (1) the widespread occurrence of partially modified and disintegrated exogenic enclaves and (2) small-scale heterogeneities in initial Sr isotope ratios as observed, for example, in sample G10 (Table 3, Fig. 4d). The higher $^{87}Sr/^{86}Sr(I)$ value (0.71146) for plagioclase compared to 0.71058 for the bulk rock system may be attributed to the incorporation of incompletely molten crustal rocks with initial $^{87}Sr/^{86}Sr$ ratios higher than that of the (crystallizing) magma. An alternative model is an origin by partial melting of a heterogeneous source and entrainment of restitic plagioclase rich in radiogenic Sr.

Origin of microgranular enclaves

Field relationships and petrographic evidence suggest that the hornblende-bearing microdioritic to microtonalitic enclaves originated from globules of mafic magma which mingled with and chilled against the host granite magma. Both the granodioritic rims of large zoned enclaves and the smaller coarse-grained tonalitic enclaves that bear textural evidence for the replacement of hornblende by biotite (e.g. samples Eck2 and E20d) were generated by relatively late-stage hybridization processes between the mafic and felsic magmas. Microtonalitic enclaves containing only biotite as the essential mafic phase show a large compositional spread in chemical variation diagrams (Fig. 2) excluding an origin by simple mingling and mixing processes between the dioritic and granitic magmas. This holds particularly true for the variations of ASI, P_2O_5, CaO, K_2O, Rb, U, Sr and Cr with Mg# (Fig. 2) and of molar $K_2O/(CaO + Na_2O)$ with Rb (Fig. 6e). Two of these enclaves (E14/5, E14/6) are characterized by relatively high Mg# (54.0 and 60.9, respectively; Table 2 and Fig. 2) and low $^{87}Sr/^{86}Sr(I)$ values (0.70731 and 0.70604, respectively; Table 3 and

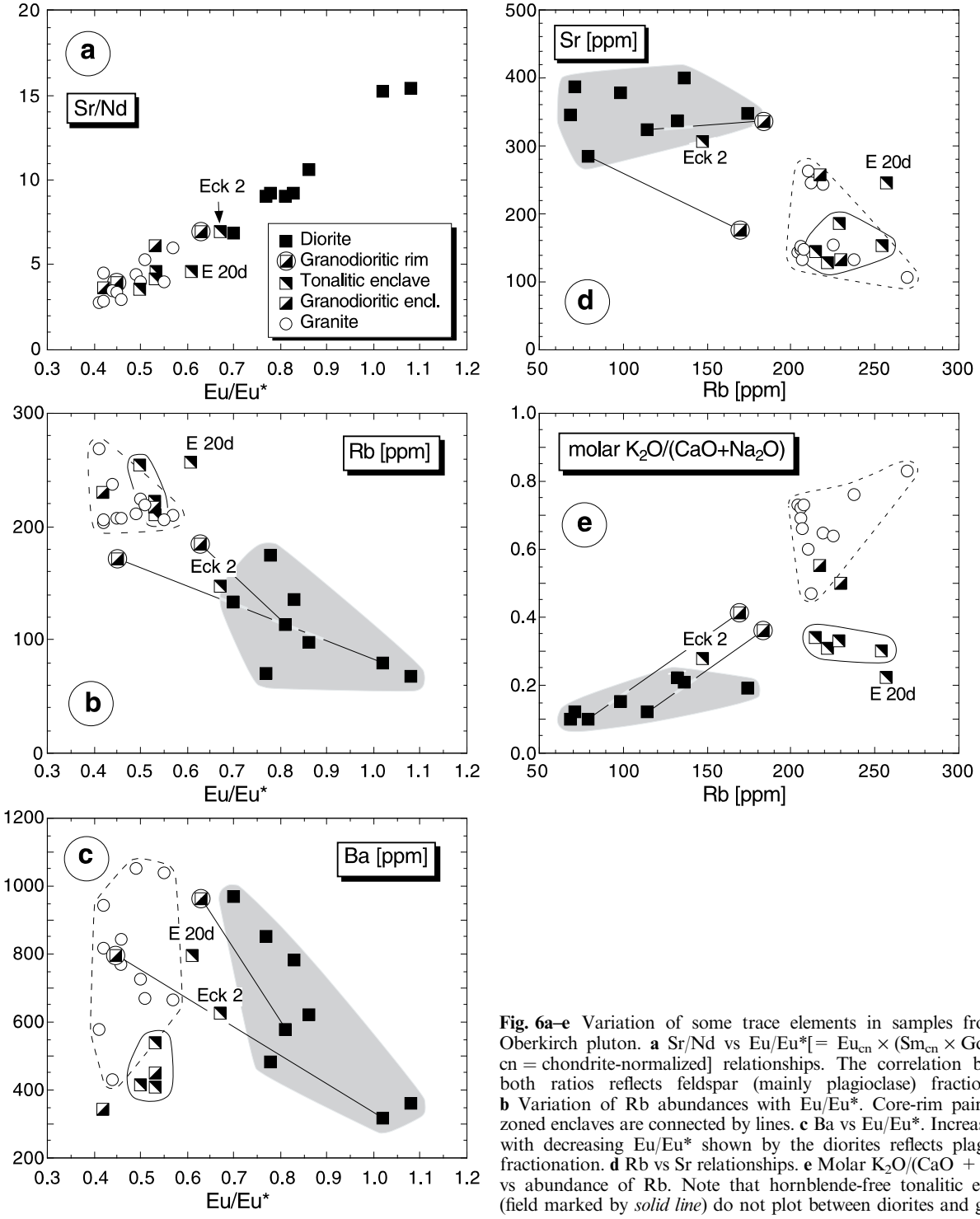

Fig. 6a–e Variation of some trace elements in samples from the Oberkirch pluton. **a** Sr/Nd vs Eu/Eu*[= $Eu_{cn} \times (Sm_{cn} \times Gd_{cn})^{-0.5}$; cn = chondrite-normalized] relationships. The correlation between both ratios reflects feldspar (mainly plagioclase) fractionation. **b** Variation of Rb abundances with Eu/Eu*. Core-rim pairs from zoned enclaves are connected by lines. **c** Ba vs Eu/Eu*. Increasing Ba with decreasing Eu/Eu* shown by the diorites reflects plagioclase fractionation. **d** Rb vs Sr relationships. **e** Molar $K_2O/(CaO + Na_2O)$ vs abundance of Rb. Note that hornblende-free tonalitic enclaves (field marked by *solid line*) do not plot between diorites and granites

Fig. 4). Since these two enclaves show fine-grained textures that are compatible with rapid crystallization caused by chilling, an origin by hybridization between dioritic magma globules and the host granitic magma is highly unlikely. Instead, these enclaves were probably formed from globules of mafic tonalitic magma unrelated to the dioritic magma globules. Some of the tonalitic enclaves showing lower Mg# and somehow more coarse-grained textures (E10g, E18k) were probably modified by hybridization processes and/or fractional crystallization.

Granodioritic enclaves that show no petrographic evidence for former existence of hornblende (e.g. samples E10sp, E18j) have chemical compositions that, in some respect, are different from those of the granodioritic rims of zoned enclaves. Their relative positions in variation diagrams, particularly in those of Al_2O_3, ASI, CaO, K_2O, Rb with Mg# (Fig. 2), suggest

an origin by hybridization between tonalitic magma globules (as represented by samples E14/6 and E14/5) and the host granitic magma.

The resorbed nature of Ab-rich cores of plagioclase megacrysts occurring in many enclaves and the similarity in An contents between these cores and many host rock plagioclase crystals suggest a common origin. Most probably, plagioclase, together with K-feldspar and quartz megacrysts from the granitic host magma were mechanically transferred to the mafic globules during the hybridization process.

Synplutonic dioritic dike and hybrid zone

The hybrid zone (~40 cm thick) between a synplutonic dike (~6 m thick) and the host granite was investigated in more detail. Ri1 represents a sample from the central part of the dike but GRi2 and G700 are granite samples taken from a distance approximately 1 m from the contact. Samples Ri8 and Ri4 were taken from the hybrid zone between the dioritic dike and the host granite. Ri8 represents the hybrid diorite-containing material from the granite as indicated by fragments and complete replacement of pyroxene and hornblende by biotite. The sample Ri4 is a granite containing fine-grained dioritic material intruded along grain boundaries. Figure 7 shows the chemical variations across the contact zone. While the major elements follow expected variation trends, P and the trace elements (e.g. Th, U, Nb, Zr, REE, Ni, Sc) do not follow a simple mixing-mingling relationship. This suggests that, in addition to mechanical mass transfer, more complex processes, such as

Fig. 7 Composition of hybrid zone between synplutonic dioritic dike (Ri1) and host granite (samples GRi2 and G700). Horizontal axis represents relative positions. See text for further explanation

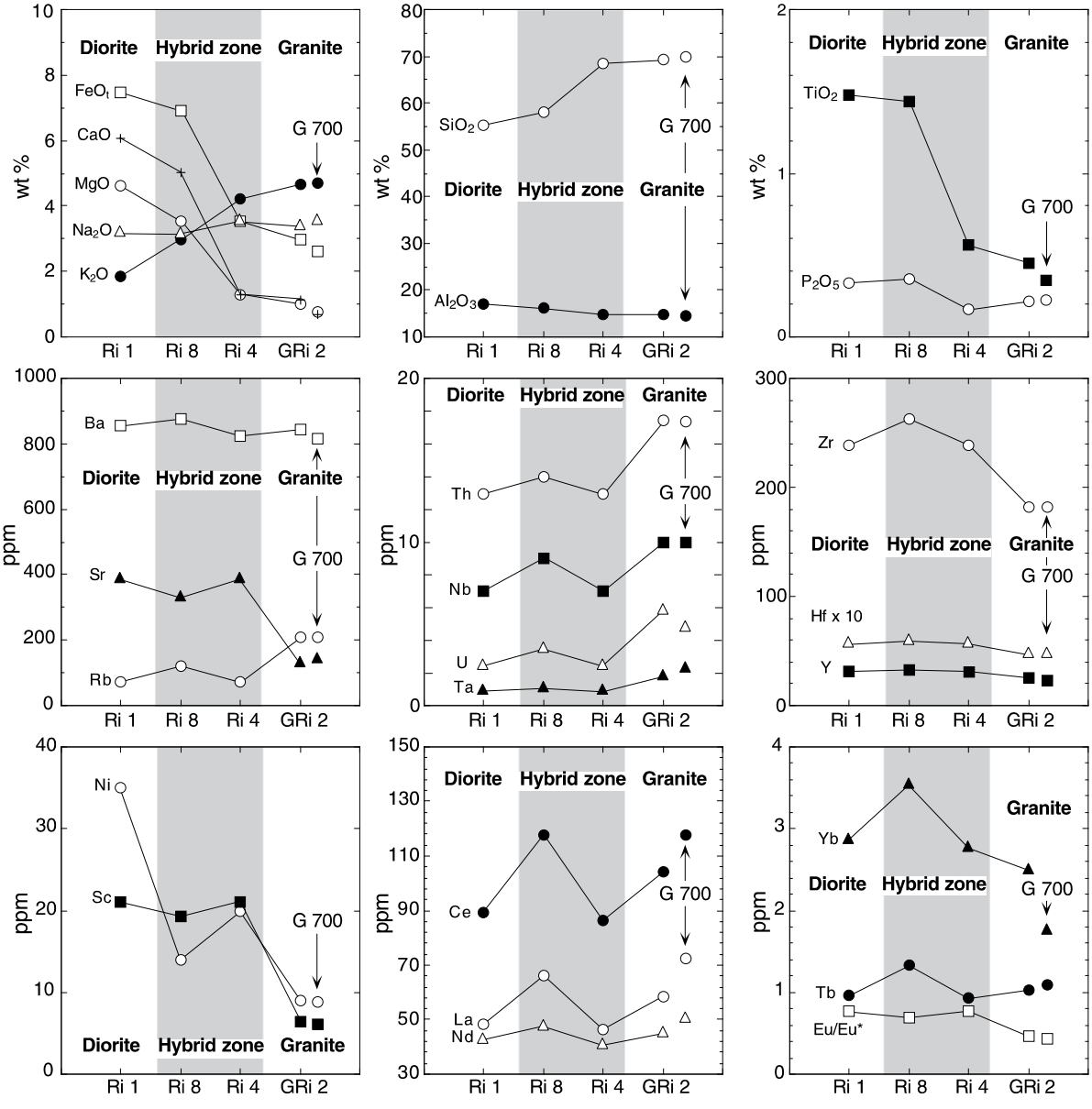

diffusion and phase reactions, were involved as indicated by petrographic evidence.

Chemical and isotopic diversity of diorites

In chemical variation diagrams, samples from the hornblende-bearing microdioritic to microtonalitic enclaves and the synplutonic dike form continuous trends that could be interpreted as liquid lines of descent with olivine, clinopyroxene, hornblende and plagioclase as major fractionating phases (Fig. 2). Plagioclase fractionation is documented by the strong positive correlation between Sr/Nd and Eu/Eu* ratios (Fig. 6a) and the decrease in Sr/Nd (and Eu/Eu*) with Mg# (Fig. 2). A simple comagmatic relationship between the diorite samples is, however, at variance with the isotopic diversity displayed by these samples (Fig. 4a–c).

The relatively wide range of isotopic data shown by the diorites may result from complex mass exchange processes between mafic globules and the felsic host magma. In principle, the mechanical incorporation of small amounts of crystals from the host granite magma as evidenced by the rare occurrence of quartz and K-feldspar megacrysts and the presence of corroded, more Ab-rich cores in plagioclase megacrysts may have slightly modified the isotopic characteristics of the enclave cores, in particular their Rb-Sr isotope systematics. However, it is highly unlikely that this process caused the large spread in $\varepsilon_{Nd}(I)$ values (−1.2 to −5.1). Melt infiltration from the host granite could also extensively modify enclave compositions (e.g. Petford et al. 1996) but the microdioritic enclaves do not bear textural evidence for such a mechanism.

From both natural examples and experiments there is ample evidence that isotopic exchange between coexisting mafic and felsic magmas can proceed much more rapidly than chemical exchange (e.g. Baker 1989; Holden et al. 1991; Van der Laan and Wyllie 1993; Lesher 1990, 1994; Elburg 1996), but as textures of the diorites suggest rapid cooling and crystallization, isotopic exchange during and after commingling should have played a subordinate role. As self-diffusion of Sr is much faster than that of Nd (Lesher 1994), significant isotopic exchange between mafic globules and felsic host should result in a relatively narrow range of initial Sr isotope ratios of the enclaves, while $\varepsilon_{Nd}(I)$ values may still be very different. This is not the case for the Oberkirch microdioritic enclaves (Fig. 4a). On the Other hand, large differences in isotopic characteristics exist between microdioritic cores and hybrid granodioritic rims of zoned enclaves (Fig. 4a). Note, for example, that the $\varepsilon_{Nd}(I)$ values of samples Hes1 (microdioritic core) and Hes1a (hybrid granodioritic rim) are almost identical (−5.1 and −5.6, respectively), while their $^{87}Sr/^{86}Sr(I)$ values are very different (0.70664 versus 0.70906, respectively). Furthermore, the sample Ri1 from the synplutonic dioritic dike shows a relatively low $\varepsilon_{Nd}(I)$ value (−4.6) that is certainly not due to isotopic exchange between the chilled mafic magma and the neighboring almost solidified granite (sample GRi2; $\varepsilon_{Nd}(I) = -6.3$). Also, in this case, initial Sr isotope ratios of the two samples are still very different (0.70690 versus 0.70947, respectively).

We conclude that the large variation in Nd-Sr isotopic characteristics displayed by the Oberkirch diorites does not result from in-situ commingling and hybridization between mafic and felsic magmas. Instead, the observed isotopic diversity may be caused by (1) source rock heterogeneities, (2) pre-commingling hybridization processes such as assimilation and combined fractional crystallization (AFC; DePaolo 1981) or (3) magma mixing. These models may be evaluated by checking for possible covariations between chemical and isotopic parameters. As can be seen from Fig. 8, isotopic variations appear to be unrelated to chemical variation. Although there is a weak negative correlation between $\varepsilon_{Nd}(I)$ and Mg# (Fig. 8a), neither $^{87}Sr/^{86}Sr(I)$ nor $\delta^{18}O$ are correlated with Mg#. If the hydrothermally altered samples Ri1 and Hes1 are excluded, $\delta^{18}O$ is nearly constant over the whole range of Mg# (∼60 to 46; Fig. 8c). It is, therefore, highly unlikely that the observed chemical variations (Fig. 2) of the diorites were caused by hybridization between mafic low-$\delta^{18}O$ and felsic high-$\delta^{18}O$ magmas or by AFC processes. As an alternative explanation, we favor an origin of the dioritic magmas by partial melting of a heterogeneous source with subsequent differentiation under low pressures within the stability field of plagioclase.

Crustal versus mantle origin of dioritic magma

Several experimental studies (e.g. Beard and Lofgren 1991; Rapp et al. 1991; Winther and Newton 1991; Wolf and Wyllie 1991, 1994; Wyllie and Wolf 1993; Sen and Dunn 1994; Patiño Douce and Beard 1995; Rapp 1995; Rapp and Watson 1995) have shown that extremely high temperatures (≥1100 °C) are needed to produce mafic metaluminous low-silica (<56 wt%) melts by dehydration melting of various metabasaltic compositions. Such melts are generally characterized by low Mg# (<44) and high contents of Na_2O (>4.3 wt%). Such features are not shown by the diorites from the Oberkirch pluton. Their REE_{cn} patterns with low $(Tb/Yb)_{cn}$ ratios (Fig. 3c) as well as high abundance of Sc, Y and Yb preclude the involvement of substantial amounts of garnet as a residual or fractionating phase. Therefore, the generation of the dioritic magmas by partial melting of mafic crustal rocks would imply that temperatures in excess of 1100 °C were reached at a depth of less than about 35 km (corresponding to the appearance of garnet in mafic rock systems at pressures above 1 GPa, Rapp and Watson 1995). Such high geothermal gradients have to be regarded as unlikely, since they would imply almost complete melting of the lower and middle crust. We, therefore, suggest that the dioritic magmas were

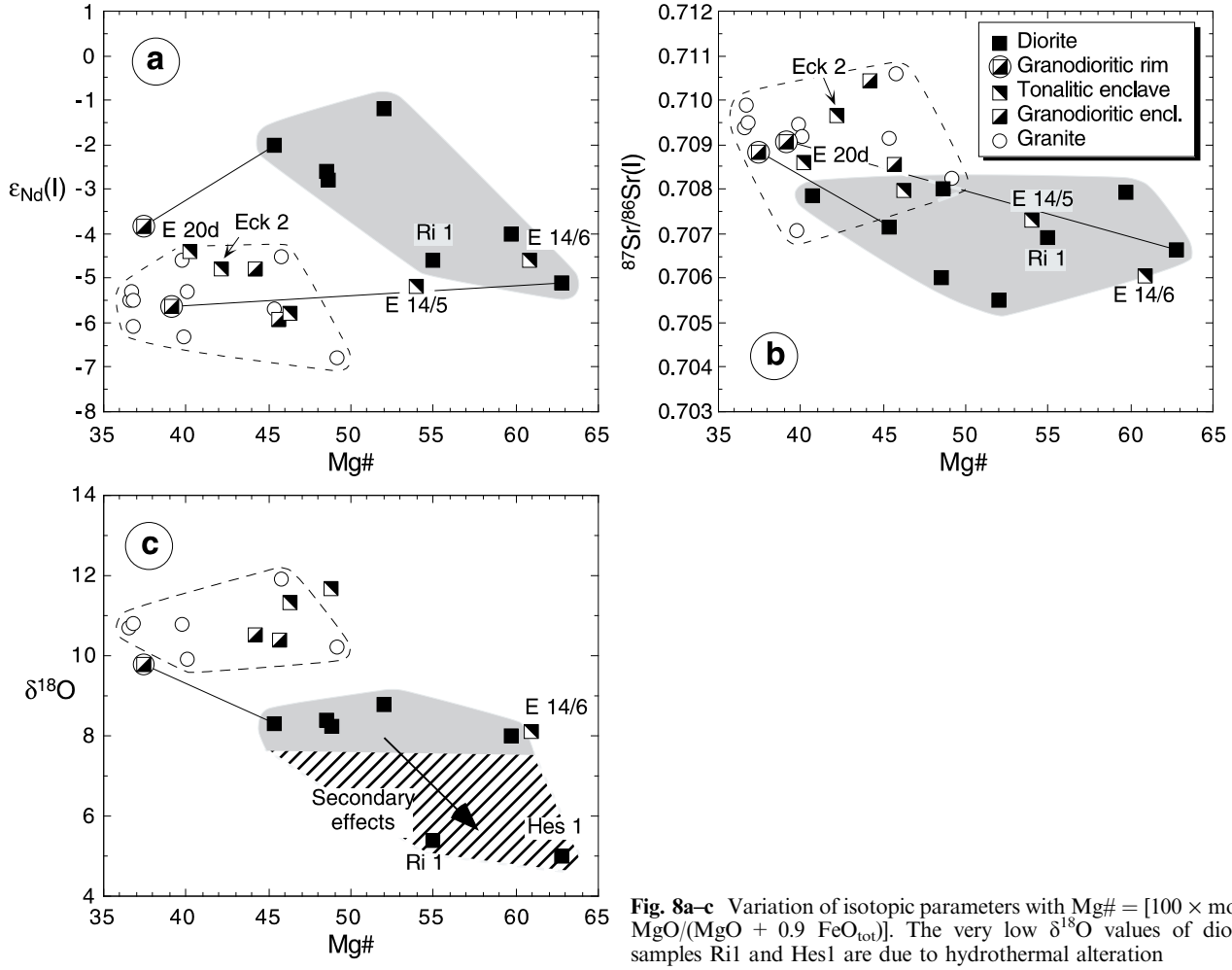

Fig. 8a–c Variation of isotopic parameters with Mg# = [100 × molar MgO/(MgO + 0.9 FeO_{tot})]. The very low $\delta^{18}O$ values of diorite samples Ri1 and Hes1 are due to hydrothermal alteration

derived from enriched lithospheric mantle sources characterized by variable Nd-Sr isotopic characteristics.

In the northern Schwarzwald, the occurrence of dioritic rocks with enriched initial Sr isotope signatures is not restricted to the Oberkirch pluton. Similar rocks forming dike-like bodies within migmatites and gneisses of the CSGC have also been found in the Rotmurg valley about 5 km to the east of the Oberkirch pluton (Von Drach and Lippolt 1974).

Origin of tonalitic magma

It has been pointed out above that the hornblende-free microtonalitic enclaves are chemically different from both the hornblende-bearing diorites and the granites (Figs. 2, 5, 6). Isotopic signatures of the least fractionated microtonalite sample E14/6 are similar to those of the low-ε_{Nd}(I) diorites that are characterized by high Mg# (Figs. 4, 8). These characteristics exclude an origin of the tonalitic magmas by thorough mixing between dioritic and granitic magma. As sample E14/6 contains plagioclase characterized by high $^{87}Sr/^{86}Sr$(I) values (Fig. 4), assimilation of crustal material by a mantle-derived melt accompanied by fractional crystallization at deeper levels of the crust appears to be a viable process for the origin of the tonalitic magmas. This model explains the elevated abundances of K, Rb, Th and U (Fig. 2) as well as the low ratios of CaO/(MgO + FeO_{tot}) (Fig. 5). Furthermore, it accounts for the fact that the chemical composition of the sample E14/6 does not match any melt composition produced experimentally by either dehydration melting of various mafic rocks or by partial melting of mantle rocks.

Conclusions

The composite Oberkirch pluton was formed by multiple intrusions of compositionally different magmas. At the exposure level, at least three main pulses of granitic magma mingled with mafic dioritic and tonalitic magma have been identified. Rapid cooling and crystallization of the dioritic and tonalitic magmas helped to preserve chemical and isotopic disequilibrium among the commingled mafic and felsic magmas. In-situ hybridization

between the magmas was limited and resulted in the formation of tonalitic to granodioritic rims around dioritic enclave cores and of smaller enclaves and schlieren. Late injection of dioritic magma into almost solidified granitic rock resulted in the formation of dioritic dike-like bodies surrounded by relatively narrow hybrid zones.

The dioritic magmas were most probably derived by partial melting from an isotopically heterogeneous, variably enriched lithospheric mantle source and subsequent fractionation of olivine, clinopyroxene, hornblende and plagioclase. Some of these magmas were modified by assimilation and incorporation of crustal material characterized by higher $^{87}Sr/^{86}Sr$ ratios resulting in mafic tonalitic compositions. The granitic magmas originated by partial melting of a heterogeneous metapelitic source and subsequent assimilation accompanied by fractional crystallization.

Acknowledgements Critical reviews by A.B. Woodland, W.E. Stephens and U. Kramm helped to improve important aspects of this paper. H. Frohna-Binder, R. Gehann (University of Karlsruhe) and H.-P. Meyer (Heidelberg) carried out the chemical analyses. Sm-Nd isotope analyses were performed by I. Deneke and H. Schyroki (Hannover) and O isotope analyses were done by A. Matthews (The Hebrew University of Jerusalem) and S. Fortier (Tübingen). This paper is a contribution from the research program 'Orogenic processes, their quantification and simulation in the Variscan belt' funded by the Deutsche Forschungsgemeinschaft (grant Al 166/8).

References

Altherr R, Henjes-Kunst F, Matthews A, Friedrichsen H, Hansen BTH (1988) O-Sr isotopic variations in Miocene granitoids from the Aegean: evidence for an origin by combined assimilation and fractional crystallization. Contrib Mineral Petrol 100: 528–541

Baker DR (1989) Tracer versus trace element diffusion: diffusional decoupling of Sr concentration from Sr isotope composition. Geochim Cosmochim Acta 53: 3015–3023

Barbarin B, Didier J (1992) Genesis and evolution of mafic microgranular enclaves through various types of interaction between coexisting felsic and mafic magmas. Trans R Soc Edinb: Earth Sci 83: 145–153

Beard JS, Lofgren E (1991) Dehydration melting and water-saturated melting of greenstone and amphibolite at 1, 3 and 6.9 kb. J Petrol 32: 365–401

Beard JS, Lofgren E, Sinha AK, Tollo RP (1994) Partial melting of apatite-bearing charnockite, granulite, and diorite: melt compositions, restite mineralogy and petrologic implications. J Geophys Res 99: 21591–21603

Boynton WV (1984) Cosmochemistry of the rare earth elements: meteorite studies. In: Henderson P (ed) Rare earth element geochemistry. Elsevier, Amsterdam, pp 63–114

Carroll MR, Wyllie PJ (1990) The system tonalite-H_2O at 15 kbar and the genesis of calc-alkaline magmas. Am Mineral 75: 345–357

Class C, Altherr R, Volker F, Eberz G, McCulloch MT (1994) Geochemistry of Pliocene to Quaternary alkali basalts from the Huri Hills, northern Kenya. Chem Geol 113: 1–22

Clayton RN, Mayeda TK (1963) The use of bromine pentafluoride in the extraction of oxygen from oxides and silicates for isotopic analysis. Geochim Cosmochim Acta 27: 43–52

Conrad WK, Nicholls IA, Wall VJ (1988) Water-saturated and undersaturated melting of metaluminous and peraluminous crustal compositions at 10 kbar: evidence for the origin of silicic magmas in the Taupo Volcanic Zone, New Zealand, and other occurrences. J Petrol 29: 765–803

DePaolo DJ (1981) Trace element and isotopic effects of combined wallrock assimilation and fractional crystallization. Earth Planet Sci Lett 53: 189–202

Eisbacher GH, Lüschen E, Wickert F (1989) Crustal-scale thrusting and extension in the Hercynian Schwarzwald and Vosges, central Europe. Tectonics 8: 1–21

Elburg MA (1996) Evidence of isotopic equilibration between microgranitoid enclaves and host granodiorite, Warburton Granodiorite, Lachlan Fold Belt, Australia. Lithos 38: 1–22

Faul H, Jäger E (1963) Ages of some granitic rocks in the Vosges, the Schwarzwald, and the Massif Central. J Geophys Res 68: 3293–3300

Gardien V, Thompson Ab, Grujic D, Ulmer P (1995) Experimental melting of biotite + plagioclase + quartz ± muscovite assemblages and implications for crustal melting. J Geophys Res 100: 15581–15591

Hanel M, Montenari M, Kalt A (1999a) Determining sedimentation ages of high-grade metamorphic gneisses by their palynological record: a case study in the northern Schwarzwald (Variscan Belt, Germany). Int Journ Earth Sciences J Earth Sci 88: 49–59

Hanel M, Kober B, Kalt A, Montenari M, Wimmenauer W (1999b) Palynomorphs and single zircon ages from paragneisses of the Schwarzwald (SW Germany): constraints on sedimentation ages. Terra Nostra 99/1: 94–95

Holden P, Halliday AN, Stephens WE, Henney PJ (1991) Chemical and isotopic evidence for major mass transfer between mafic enclaves and felsic magma. Chem Geol 92: 135–152

Kalt A, Grauert B, Baumann A (1994a) Rb-Sr and U-Pb isotope studies on migmatites from the Schwarzwald (F.R.G.): constraints on isotopic resetting during Variscan high-temperature metamorphism. J Metamorph Geol 12: 667–680

Kalt A, Hanel M, Schleicher H, Kramm U (1994b) Petrology and geochronology of eclogites from the Variscan Schwarzwald (F.R.G.). Contrib Mineral Petrol 115: 287–302

Kalt A, Hanel M, Wimmenauer W (1999) Tectonometamorphic units in the Schwarzwald. Terra Nostra 99/1: 116

Kossmat F (1927) Gliederung des varistischen Gebirgsbaus. Abh Sächs Geol Landesamt 1: 1–39

Le Breton N, Thompson AB (1988) Fluid-absent (dehydration) melting of biotite in metapelites in the early stages of crustal anatexis. Contrib Mineral Petrol 99: 226–237

Lesher CE (1990) Decoupling of chemical and isotopic exchange during magma mixing. Nature 344: 235–237

Lesher CE (1994) Kinetics of Sr and Nd exchange in silicate liquids: theory, experiments, and applications to uphill diffusion, isotopic equilibration, and irreversible mixing of magmas. J Geophys Res 99: 9585–9604

Lippolt HJ, Hradetzky H, Hautmann S (1994) K-Ar dating of amphibole-bearing rocks in the Schwarzwald, SW Germany: I. $^{40}Ar/^{39}Ar$ age constraints to Hercynian HT-metamorphism. Neues Jahrb Mineral Monatsh 1994: 433–448

Mezger K, Altherr R, Okrusch M, Henjes-Kunst F, Kreuzer H (1985) Genesis of acid/basic rock associations: a case study. The Kallithea intrusive complex, Samos, Greece. Contrib Mineral Petrol 90: 353–366

Otto J (1971/72) Der Granit von Oberkirch im Nordschwarzwald. Ber Naturf Ges Freiburg i Br 61/62: 5–57

Otto J (1974) Die Einschlüsse im Granit von Oberkirch (Nordschwarzwald). Ber Naturf Ges Freiburg i Br 64: 83–174

Patiño Douce AE (1996) Effects of pressure and H_2O content on the composition of primary crustal melts. Trans R Soc Edinb: Earth Sci 87: 11–21

Patiño Douce AE, Beard JS (1995) Dehydration-melting of biotite gneiss and quartz amphibolite from 3 to 15 kbar. J Petrol 36: 707–738

Patiño Douce AE, Beard JS (1996) Effects of P, $f(O_2)$ and Mg/Fe ration on dehydration melting of model metagreywackes. J Petrol 37: 999–1024

Patiño Douce AE, Johnston AD (1991) Phase equilibria and melt productivity in the pelitic system: implications for the origin of peraluminous granitoids and aluminous granulites. Contrib Mineral Petrol 107: 202–218

Petford N, Paterson B, McCaffrey K, Pugliese S (1996) Melt infiltration and advection in microdiorite enclaves. Eur J Mineral 8: 405–412

Poli GE, Tommasini S (1991) Model for the origin and significance of microgranular enclaves in calc-alkaline granitoids. J Petrol 32: 657–666

Rapp RP (1995) Amphibole-out phase boundary in partially melted metabasalt, its control over liquid fraction and composition, and source permeability. J Geophys Res 100: 15601–15610

Rapp RP, Watson EB (1995) Dehydration melting of metabasalt at 8–32 kbar: implications for continental growth and crust-mantle recycling. J Petrol 36: 891–931

Rapp RP, Watson EB, Miller CF (1991) Partial melting of amphibolite/eclogite and the origin of Archean trondhjemites and tonalites. Precambrian Res 51: 1–25

Rushmer T (1991) Partial melting of two amphibolites: contrasting experimental results under fluid-absent conditions. Contrib Mineral Petrol 107: 41–59

Sen C, Dunn T (1994) Dehydration melting of a basaltic composition amphibolite at 1.5 and 2.0 GPa: implications for the origin of adakites. Contrib Mineral Petrol 117: 394–409

Singh J, Johannes W (1996) Dehydration melting of tonalites. Part II. Composition of melts and solids. Contrib Mineral Petrol 125: 26–44

Skjerlie KP, Johnston AD (1994) Vapor-absent melting at 10 kbar of a biotite- and amphibole-bearing tonalitic gneiss: implications for the generation of A-type granites. Geology 20: 263–266

Skjerlie KP, Johnston AD (1996) Vapour-absent melting from 10 to 20 kbar of crustal rocks that contain multiple hydrous phases: implications for anatexis in the deep to very deep continental crust and active continental margins. J Petrol 37: 661–691

Skjerlie KP, Patiño Douce AE, Johnston AD (1993) Fluid absent melting of a layered crustal protolith: implications for the generation of anatectic granites. Contrib Mineral Petrol 114: 365–378

Thompson AB (1996) Fertility of crustal rocks during anatexis. Trans R Soc Edinb: Earth Sci 87: 1–10

Van der Laan SR, Wyllie PJ (1993) Experimental interaction of granitic and basaltic magmas and implications for mafic enclaves. J Petrol 34: 491–517

Vernon RH (1984) Microgranitoid enclaves: globules of hybrid magma quenched in a plutonic environment. Nature 304: 438–439

Vernon RH (1990) Crystallization and hybridism in microgranitoid enclave magmas: microstructural evidence. J Geophys Res 95: 17,849–17,859

Vielzeuf D, Holloway JR (1988) Experimental determination of fluid-absent melting relations in the pelitic relations in pelitic system. Contrib Mineral Petrol 98: 357–276

Vielzeuf D, Montel JM (1994) Partial melting of metagreywackes. 1. Fluid-absent experiments and phase relationships. Contrib Mineral Petrol 117: 375–393

Von Drach V (1978) Mineral-Alter im Schwarzwald. Thesis, University of Heidelberg, Heidelberg, Germany

Von Drach V, Lippolt HJ (1974) Herkunft eines dioritischen Gesteins des Nordschwarzwalds, gedeutet aufgrund seiner K-Rb-Sr-Eigenschaften. Neues Jahrb Mineral Abh 122: 229–245

Winther KT (1996) An experimentally based model for the origin of tonalitic and trondhjemitic melts. Chem Geol 127: 43–49

Winther KT, Newton RC (1991) Experimental melting of hydrous low-K tholeiite: evidence on the origin of Archean cratons. Bull Geol Soc Den 39: 213–228

Wolf MB, Wyllie JP (1991) Dehydration melting of solid amphibolite at 10 kbar: textural development, liquid interconnectivity and applications to the segregation of magmas. Mineral Petrol 44: 151–179

Wolf MB, Wyllie PJ (1994) Dehydration-melting of amphibolite at 10 kbar: the effects of temperature and time. Contrib Mineral Petrol 115: 369–383

Wyllie PJ, Wolf MB (1993) Amphibolite dehydration-melting: sorting out the solidus. In: Prichard HM, Alabaster T, Harris NBW, Neary CR (eds) Magmatic processes and plate tectonics. Geol Soc Lond Spec Publ No 76: 405–416

Wyllie PJ, Cox KG, Biggar GM (1962) The habit of apatite in synthetic systems and igneous rocks. J Petrol 3: 238–243

Zorpi MJ, Coulon C, Orsini JB, Cocirta C (1989) Magma mingling, zoning and emplacement in calc-alkaline granitoid plutons. Tectonophysics 157: 315–329